Cellulose-based Scaffolds for Lithium Capturing

Jeffrey Hsu

A thesis

submitted in partial fulfillment of the

requirements for the degree of

Master of Science

University of Washington

2022

Committee:

Eleftheria Roumeli

Chinmayee Subban

Program Authorized to Offer Degree*:*

Department of Materials Science and Engineering

University of Washington

Abstract

Cellulose-based Scaffolds for Lithium Capturing

Jeffrey Hsu

Chair of the Supervisory Committee:

Prof. Eleftheria Roumeli

Department of Materials Science and Engineering

Cellulose, a naturally occurring and most abundant bio-based polymer on earth. It offers flexibility when it comes to potential applications in various industries and has been continued to be modified to fit such demands. Obtaining cellulose from different sources, or processing cellulose to alter its chemical structure are strategies that offer control of the final material performance and can lead to vastly different properties. Ultimately, cellulose is a material that is both widely available and capable of fulfilling the needs of numerous markets and industries. One of the key advantages of cellulose is its hierarchical structure that gives rise to exceptional mechanical properties, among other features. Utilizing different synthesis and processing methods, different types of nanocellulose can be prepared. These include crystalline nanocellulose, cellulose nanofibrils and bacterial cellulose.

Here we explore the potential use of nanocellulose as a matrix material for nanocomposite membranes aiming to capture Li ions from seawater. We choose nanocellulose as it combines high strength and porosity and is derived from renewable resources. While cellulose itself is not selective for Li ions, non-toxic Hydrogen Titania Oxide (HTO) nanoparticles serving as a filler for the nanocomposite membranes presented in this work offer Li selectivity, and can be used in conjunction with nanocellulose to form a proper platform for Li capturing. Here, we prepare several different cellulose scaffolds and compare them as matrix materials for HTO nanoparticles with the key criteria for our evaluation being the structural stability and reusability

of the membrane. Matrix materials studied include crystalline and nanofibril hydrogels along with bacterial cellulose films that have been either retained in their original state or freeze-dried to increase porosity.

University of Washington
Graduate School

This is to certify that I have examined this copy of a master's thesis

by: Jeffrey Hsu

And have found it complete and satisfactory in all respects,

and that any and all revisions required by the

final examining committee have been made.

Committee Members:

_____

Prof. Eleftheria Roumeli

_____

Prof. Chinmayee Suban

Date: _____

In presenting this thesis in partial fulfillment of the requirements for a master's degree at the University of Washington, I agree that the library shall make its copies freely available for inspection. I further agree that extensive copying of this dissertation is allowable only for scholarly purposes, consistent with "fair use" as prescribed in the U.S Copyright Law. Any other reproduction for any purposes or by any means shall not be allowed without my written permission.

Signature: _____

Date: _____

Table of Contents

List of Figures

List of Tables

ACKNOWLEDGEMENTS

I would like to thank everyone who has supported me in this long journey. First and foremost, my family, who continues to give me the confidence I need throughout these difficult times. I would also like to thank my advisor, Dr. Eleftheria Roumeli, who has guided and inspired me throughout my Masters career. In addition, I also thank our partners in this project, Dr. Chinmayee Subban from the Pacific Northwest National Lab. the members of our group that have contributed to my project including Jeremy Fredericks, Andrew Jimenez, Esther Law, Konstantina Mason, and Elisabeth Ryan.

Chapter 1– Introduction

1.1 Motivation

The significant industrial relevance of lithium (Li) to sectors including energy, transportation, telecommunications and aerospace, primarily due to its use in rechargeable batteries, has been driving research for its recovery from viable resources, including seawater, waste batteries and industrial wastewater [1]. Oceans contain approximately 2.6×10^{11} tons of Li, but the exceedingly low concentrations make extraction from seawater incredibly challenging. In addition, the scale and amount of Li captured per cycle per unit of biocomposite also needs to be factored if this solution is to be economically-viable and sustainable [2]. Strategies to recover Li ions from seawater include adsorption, membrane distillation, solvent extraction, ion exchange resins and co-precipitation [3]. Currently, there is effort in researching economically-viable and practical solutions to develop cellulose-based scaffolds as a way to extract Li ions efficiently [4].

In order to maintain a renewable and environmentally-friendly stance in this topic of interest, cellulose-based composites will be focused along with benign and non-toxic nanoparticles that will be highly selective for Li ions. This thesis will explore several different methods in order to test which is most efficient in infiltrating the nanoparticles into the cellulose scaffolds while retaining robustness and reusability throughout multiple cycles.

1.2 Cellulose-based Biocomposites

Cellulose, the world's most abundant biopolymer, has been suggested as a polymer scaffold in such applications [5]. Cellulose combines being renewable, processable by a plethora of manufacturing methods, has excellent specific mechanical properties (higher than steel or kevlar fibers), and is also bio-compatible, thus eliminating the risk of pollution if deployed in the ocean [4]. Cellulose is composed of numerous glucose molecules connected by beta glycosidic

bonds that form long chains and are mainly found in lignocellulosic biomass such as trees, reeds, plant stock, and algae [6]. Cellulose is also found with hemicellulose, lignin and other extractives that form the overall plant cells. The fibers themselves are aggregated together via Van Der Waals forces along with inter and intra-fibril Hydrogen bonding [7]. To isolate the cellulose fibers, a series of chemical pretreatment needs to be done on the starting biomass. This will mainly fractionalize the biomass into three components; cellulose, hemicellulose and lignin [8]. The cellulose will be further bleached to remove residue lignin in order to obtain as pure of cellulose as possible. Removing impurities will help increase mechanical properties [9]. Capitalizing on the versatility of cellulose, the goal is to prepare porous polymer structures with uniformly distributed HTO nanoparticles and investigate their efficiency for reversible Li+ capture from seawater [10]. The distinguishing feature of nanocellulose is the dimensions of individual cellulosic particles that gives it superior properties over unmodified cellulose [11]. One of the main advantages of utilizing cellulose in the nanoscale scale is the sheer amount of Hydrogen bonding that occurs on that scale due to the increase in surface area that significantly changes the mechanical properties. They also serve well as reinforcement materials in composites thanks to their size [12]. In addition, there are multiple types of nanocellulose with varying properties that can be modified to fit various applications. The most common being cellulose nanocrystals (CNC), cellulose nanofibrils (CNF), and bacterial nanocellulose (BC). One common attribute between all three different types of nanocellulose is that they are mostly crystalline or amorphous regions of cellulose fibers in polymeric bundles on the nanoscale. Additionally, all nanocellulose derivatives are highly hydrophilic, meaning they will take up water very easily and create suspensions at low concentrations. Crystalline regions are more ordered and linear compared to amorphous regions which are more disordered and random. Each type of nanocellulose requires different synthesization methods that range from chemical modifications to bacterial

fermentation and will vary in mechanical property [13]. There are multiple methods to synthesize both the HTO nanoparticles and the cellulose scaffolds [14]. Cellulose hydrogels can be synthesized from various types of cellulose-derivatives. The main types focused will be CNF and BC for these series of experiments. The cellulose scaffolds will be produced via TEMPO-oxidation and mechanical defibrillation for CNF and grown via bacteria for BC [15, 16]. In addition, the cellulose hydrogels will be synthesized by incorporating metal nitrates, such as $Zn(NO_3)_2$, $Ca(NO_3)_2$, $Cu(NO_3)_2$, into the cellulose scaffolds [17].

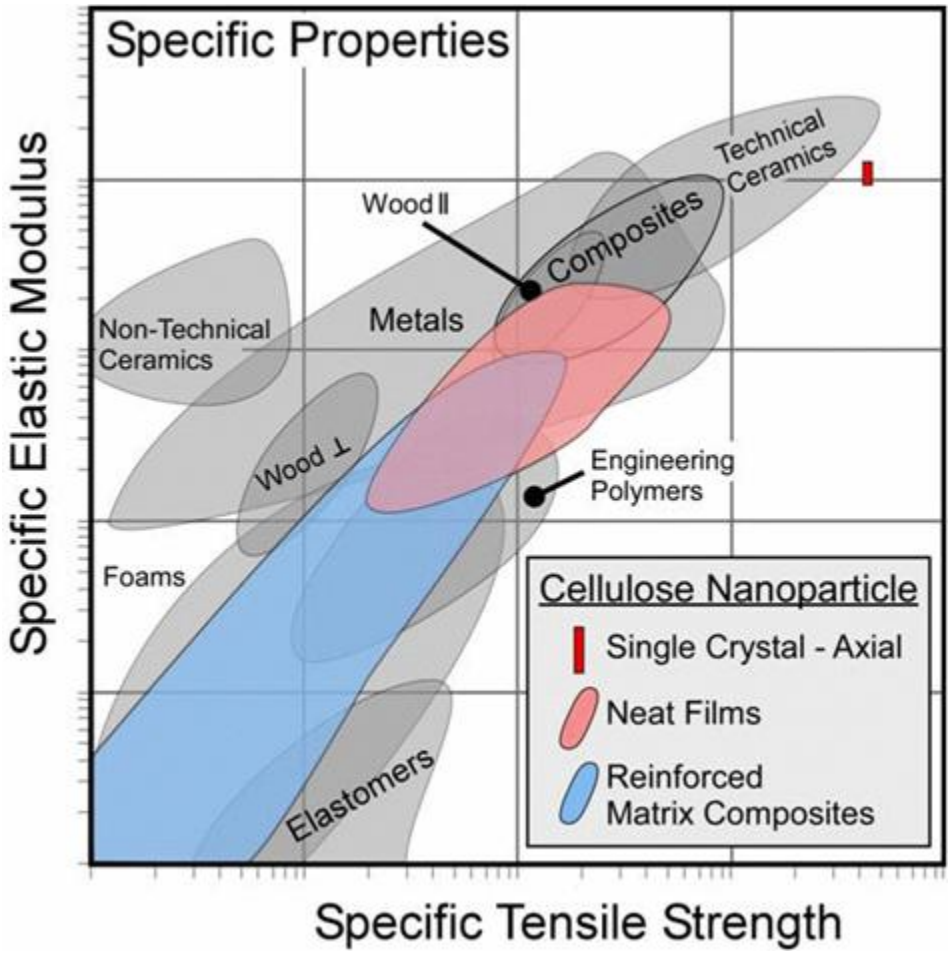

Figure 1. Specific tensile strength and elastic modulus graph of various materials. Note that a single strand of cellulose nanoparticles has one of the highest tensile strength and elastic modulus of all the materials shown. Figure adapted from [18].

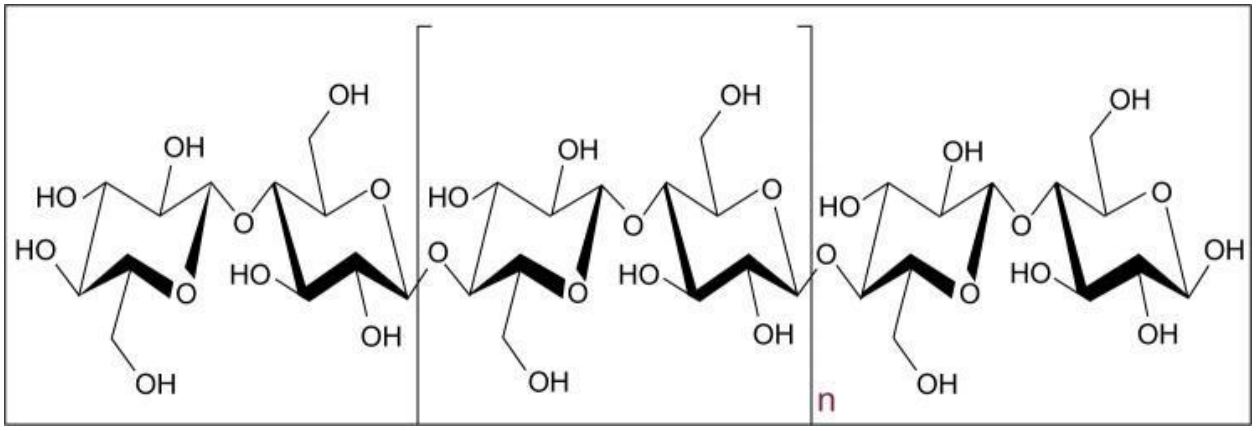

Figure 2. Chemical structure of cellulose, made up of multiple glucose molecules covalently linked with (1–4) glycosidic bonds Figure adapted from [6].

1.3 Cellulose Nanocrystals (CNC)

CNC is characterized by the low aspect ratio (L/D) of individual crystals that is extracted from the base cellulose material. Compared to other types of nanocellulose, CNC are rod or whisker shaped and dimensions will vary depending on the type of cellulose material used along with preparation method [19]. This is due to the treatment methods that primarily target amorphous regions of the cellulose so that only the crystalline regions remain intact, hence the name cellulose nanocrystals [20]. Typically CNC length will vary from 70-2000 nm and width from 3-50 nm giving CNC an aspect ratio range of 2-200 [6]. CNC can be produced from any type of cellulosic material such as wood, cotton and even sea algae [21]. There are multiple mechanical and chemical treatments to produce CNC which include cyrocrushing (freezing the cellulose fibers then crushing them to reduce size), high pressure homogenization (filtering cellulose fibers through nano-size filters using high pressure and water), and acid hydrolysis [21]. The main focus for this paper will be acid hydrolysis where the cellulose will be hydrolyzed in sulfuric acid for a set amount of time. In acid hydrolysis for CNC, processing conditions, especially temperature and reaction time, is vital for the quality of nanocrystals [22]. For example, if the reaction time is

too short, amorphous regions of cellulose could still remain which will change the overall morphology and thus the properties of that CNC sample.

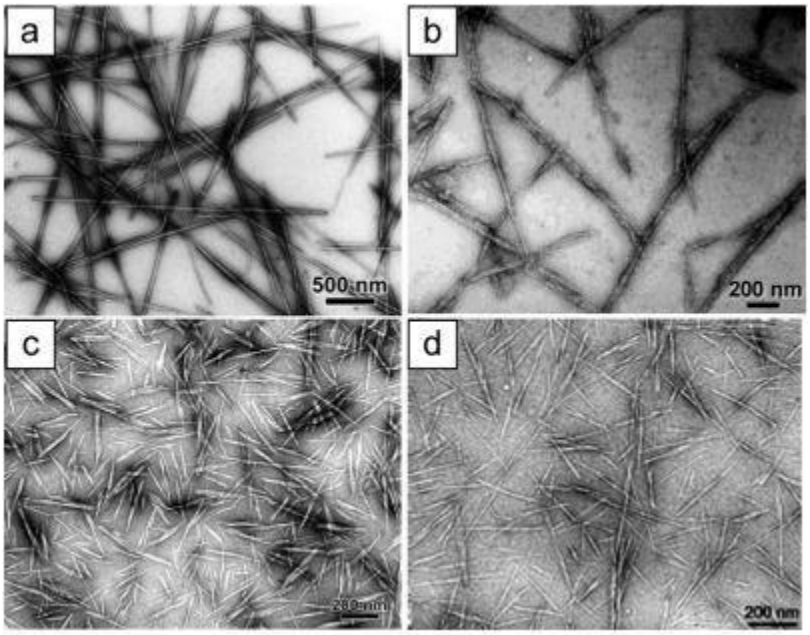

Figure 3. TEM images of dried dispersion of cellulose nanocrystals derived from (a) tunicate , (b) bacterial fermentation, (c) ramie, and (d) sisal Figure adapted from [5].

Table 1. Overview of the dimensions of cellulose nanocrystals from different sources and preparation methods. Table adapted from [6].

Source	Preparation method	Length (nm)	Width (nm)	Aspect ratio (L/D)	Reference
Wood	H_2SO_4 hydrolysis	100–300	3–5	20–100	37,45
Cotton	HCl hydrolysis	100–150	5–10	10–30	38
Ramie	H_2SO_4 hydrolysis	70–200	5–15	~12	39
Sisal	H_2SO_4 hydrolysis	100–300	3–5	~60	40
Valonia	H_2SO_4 hydrolysis	1,000–2,000	10–20	50–200	41
Tunicates	H_2SO_4 hydrolysis	>1,000	10–20	~100	42
Bacteria	H_2SO_4 hydrolysis	100–1,000	10–50	2–100	43
Bacteria	HCl hydrolysis	160–420	15–25	7–23	44

1.4 Cellulose Nanofibrils (CNF)

CNF offers much greater aspect ratios compared to CNC, partially due to the chemical pretreatments that remove crystalline regions and leaving the amorphous regions intact, which are mainly composed of fibers versus crystals particles [23]. Compared to CNC, CNF fibers typically have smaller diameters and significantly longer lengths. However, just like CNC, different production methods will play a role in the final dimensions of the CNF fibers. Diameters for CNF can range anywhere from 5-50 nanometers. Aspect ratio range for CNF can easily be over 200 due to varying lengths of the fibers that can reach over a few micrometers long [24]. CNF can also be produced with different chemical and mechanical methods including cryogrinding, ultrasonication, enzymatic hydrolysis, mechanical defibration, TEMPO oxidation or a combination of methods [25]. The main focus for this paper is producing CNF via TEMPO oxidation with mechanical defilbration. The finished product will generally be viscous liquid, almost gel-like, if concentrated enough on the macro scale; however closer inspection with an optical microscope will reveal long nanofibers bundled within the fluid. Due to the interbonding of the fibers, CNF are ideal for thin film and hierarchical structure applications [24]. This includes synthesis into an aerogel, transparent films and also hydrogels. In addition, CNF has found uses as reinforcement materials within the paper and pulp industry and use as 3D printing material. The shear thinning properties associated with CNF allows it to change viscosity depending on the amount of shear force applied to it, allowing CNF to be utilized for 3D bioprinting of structures such as aerogels [26].

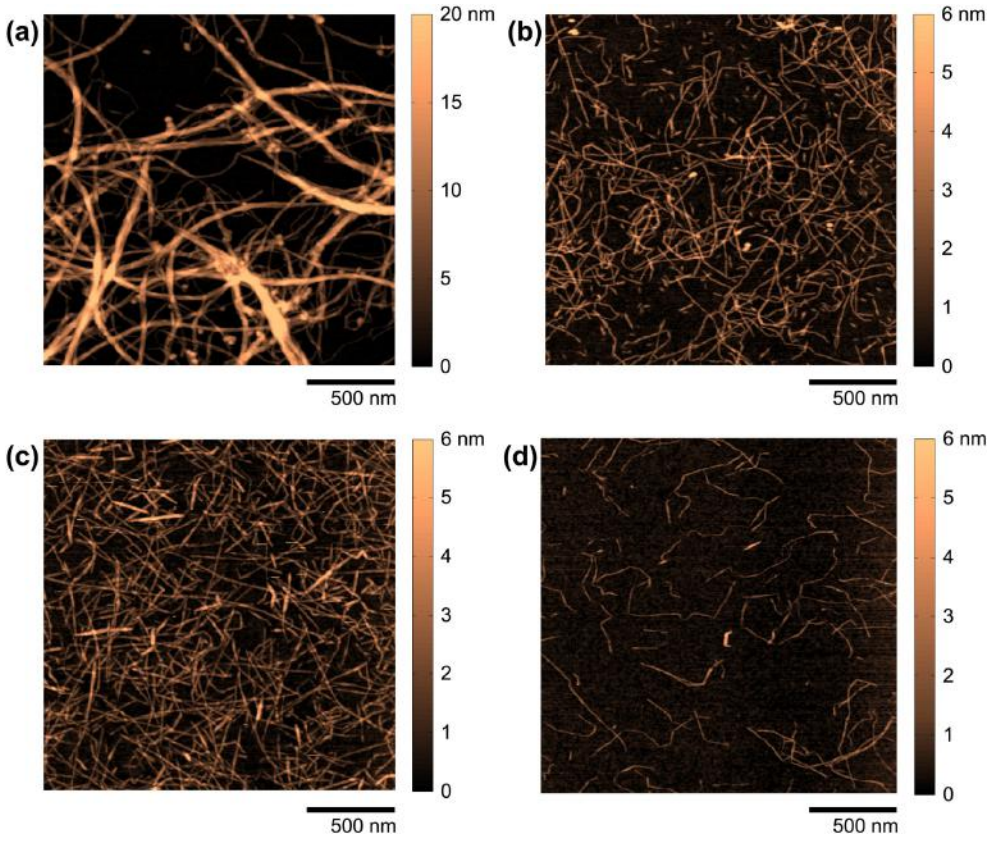

Figure 4. AFM height images of CNF, produced from hardwood kraft pulp using homogenization of: (a) non-pretreated, (b) carboxymethylated, (c) carboxylated via TEMPO-mediated oxidation or (d) quaternized cellulose. Figure adapted from [27].

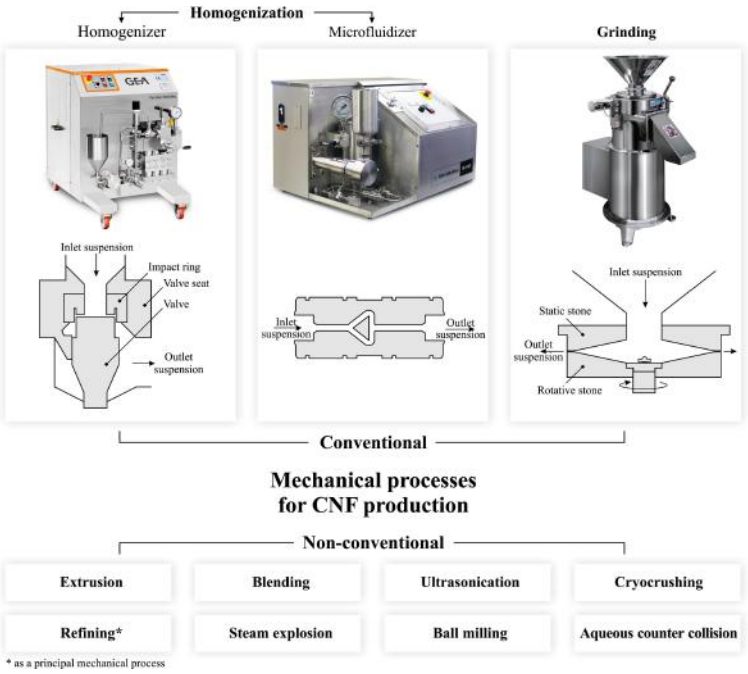

Figure 5. Different mechanical methods for CNF production. Figure adapted from [25].

1.5 Bacterial Cellulose

Bacterial cellulose is similar in morphology to CNF, the bacterial cellulose sheets are mainly long strands of cellulose nanofibers bundled together. The main difference is how it's produced. Bacterial cellulose is primarily produced via fermentation using cellulose-producing bacteria such as *Gluconacetobacter xylinus* [28]. One of the more unique properties of BC is that it can be grown to any shape desired which makes it very flexible when it comes to the end product. This is due to how BC pellicles are grown within containers or enclosements that can come in many shapes and sizes. The bacteria is suspended in a media and fed polysaccharides for it to produce cellulose. Then after approx. 30 days, the bacterial cellulose is harvested for later use [29]. This also comes with the benefits of no impurities along with a higher degree of polymerization which is the amount of monomers in the polymer chains [30]. Bacterial cellulose fibers are 1-25 nm in diameter and 1-9 um in length giving them an aspect ratio range of 100-360 [31]. Due to the non-toxic nature of BC, it has potential application in medical drug delivery systems, bandage dressings and food additives. Structurally, BC comes in hydrophilic sheets called pellicles which vary in size and have high tensile strength compared to other contemporary materials [32].

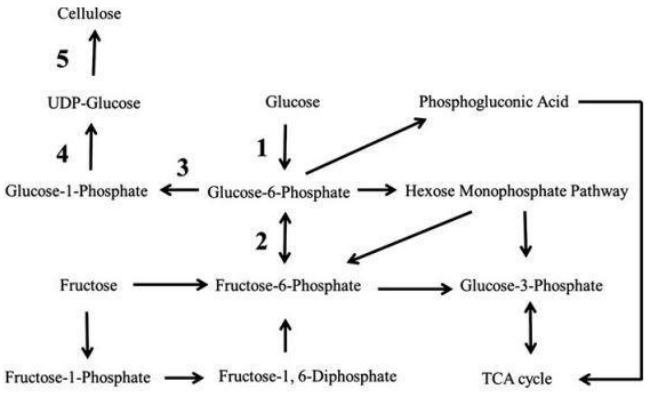

Figure 6. Pathway of bacterial cellulose synthesis from glucose in Acetobacter xylinum. (1) glucokinase, (2) isomerase, (3) phosphoglucomutase, (4) UDPG-pyrophosphorylase, (5) cellulose synthase. Figure adapted from [30].

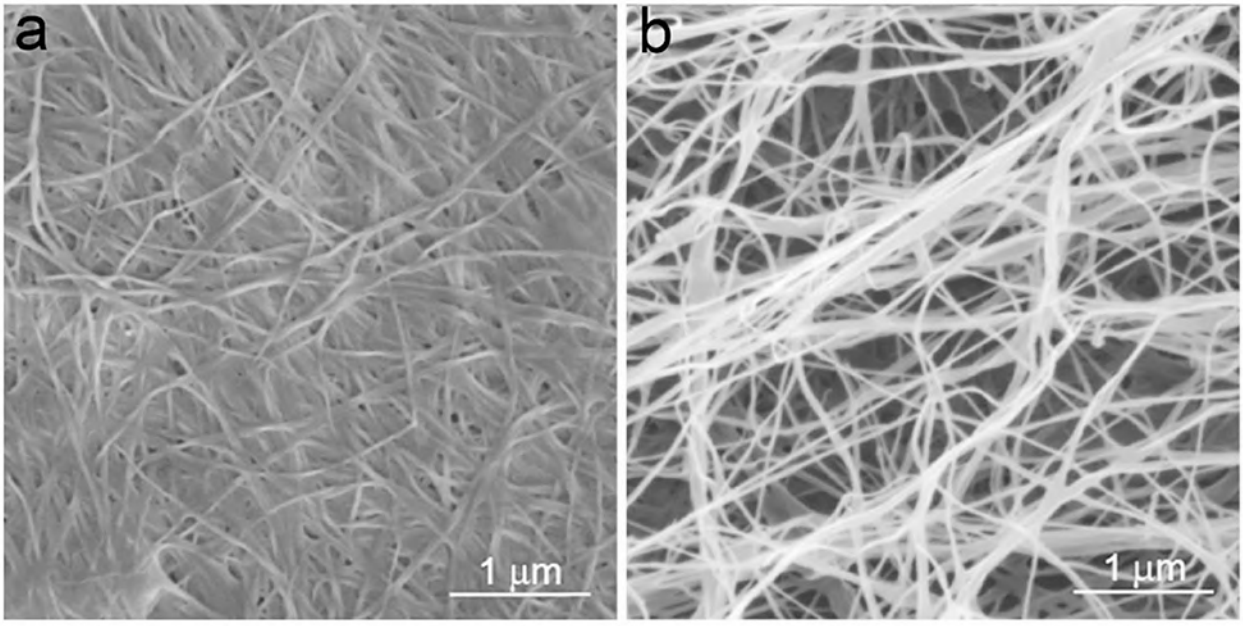

Figure 7. SEM images of BC. (a) BC pellicle harvested from static fermentation and (b) nanofibers detached from BC pellicle obtained via sonication. Figure adapted from [31].

1.6 Nanoparticles for Selectivity

Research shows very high Li^+ selectivity in several manganese and titanium oxide compounds through adsorption. These include hydrogen manganese oxide (HMO) and H_2TiO_3 (HTO) [4, 33]. Both HMO and HTO show high selectivity for Li and excellent Li-capture capabilities when embedded into cellulose films; 21.6 mg/g and 39.8 mg/g respectively. In particular, H_2TiO_3 (hereinafter HTO) being cheap, environmentally benign, highly selective for Li^+, and with promising Li-capture capacities is an attractive material to pursue [4,33]. Once the HTO is saturated, Li^+ can be recovered by regenerating with an HCl wash, where H^+ replaces Li^+ resulting in a Li-rich solution [34]. Given that HTO captures $Li+^+$ by chemisorption achieving higher capacities and reliable practical reuse requires embedding nanoparticles of HTO in a porous polymer scaffold, conventionally composed of petrochemical-derived polymers which have adverse effects on the environment [35, 36]. Analytical studies (ICP-MS) with suitable

calibration and standards will be performed to measure Li^+ capture capacities of the nanocomposite hydrogels in synthetic and natural seawater [37, 38]. Further, the sustained capacities upon regeneration will be measured by saturating the nanocomposites with $Li+^+$ using LiOH and subsequently regenerating using HCl [34]. The resulting capacity data will guide our nanocomposite optimization effort.

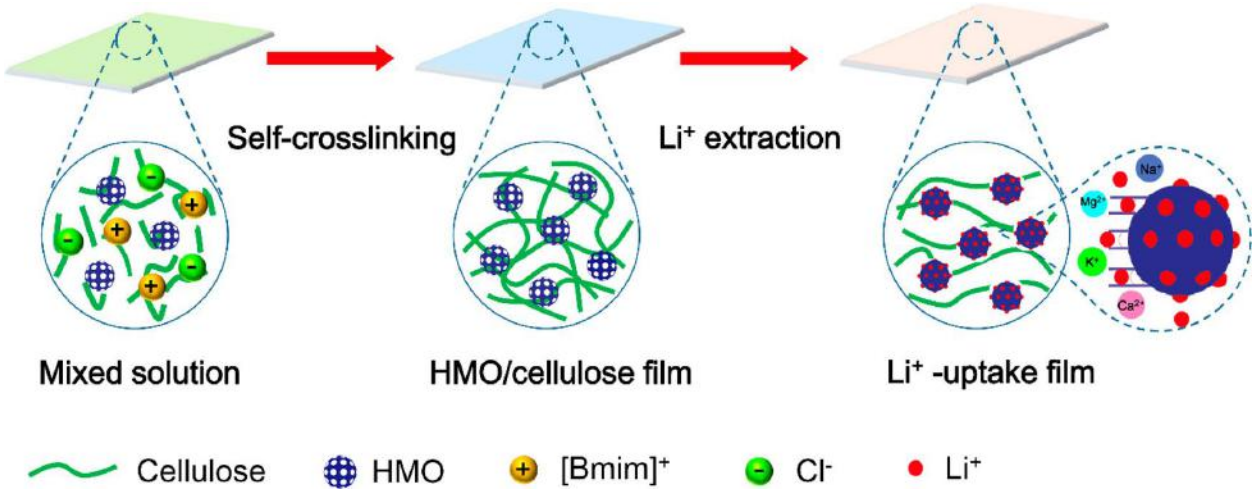

Figure 8. Schematic diagram of the preparation and structure of the HMO/cellulose film and Li+ uptake by the film. Figure adapted from [4].

1.7 Objectives

As shown before, cellulose is an abundant, renewable bioresource that is versatile and easily modified via chemical and mechanical means. Especially in the nanocellulose form, they can be adapted for more complex applications that require a combination of desirable properties such as reusability, strength, and structural morphology. This research thesis will primarily focus on the synthesis and applicability of cellulose nanocrystals, cellulose nanofibrils , and bacterial cellulose as cellulose scaffolds infiltrated with Li-selective HTO nanoparticles. These cellulose scaffolds will be assessed on the basis of robustness, reusability and nanoparticle retention. Furthermore, potential infiltration methods will also be investigated in order to assess which one

will give the best retention and infiltration of the nanoparticles into the cellulose scaffolds. Specific objectives are as followed:

1. Explore the different types of nanocellulose, successfully synthesize each type, and determine the most effective one to serve as a scaffold for HTO nanocomposite membranes
2. Determine which infiltration techniques (passive vs active) will give the best results for nanoparticle intake and retention after multiple harvesting cycles
3. Characterize the BC nanocomposites and HTO particles size using TGA (weight % of nanoparticles successfully infiltrated) and SEM (size distribution for both fibers and particles)

As these objectives are explored and results are presented, obstacles will be revealed and must be overcomed before these BC composites will be considered viable in the real world environment. This thesis will explore the experimental methodology of determining proper cellulose scaffolds and discussing the results of the BC composites in the scope of multiple factors. These results will also contribute to future research on the efficiency of the composite scaffolds in Li capturing applications.

Chapter 2 – Material and Methods

2.1 Materials

2.1.2 Cellulose Base Materials

The three different types of nanocellulose started off as different cellulose based products. For CNC, it started as alpha cellulose powder purchased from Sigma Aldrich with length and width in the micrometers. Hydroxyethyl cellulose was also purchased from Aldrich for hydrogel testing.CNF was synthesized from bleached card stock from Georgia Pacific that would later be pulped in preparation for chemical pretreatment. BC was fermented using a Symbiotic Culture of Bacteria and Yeast (SCOBY).

2.1.3 Chemicals

For CNC, 50% wt sulfuric acid, purchased from Sigma Aldrich, was used in the acid hydrolysis. CNF was pretreated with solid NaBr, TEMPO, NaClO, 1M HCl and 1M NaOH all purchased from Sigma Aldrich. $Ca(NO_3)_3$, $Zn(NO_3)_3$, and $Cu(NO_3)_3$ solid pellets were also purchased from Sigma Aldrich. BC was fermented using commercially available teabags, kombucha SCOBY starter, cane sugar and apple cider vinegar. In addition, NaOH, sourced from Sigma Aldrich, is also used to harvest the BC.

2.1.4 HTO

H2TiO3 synthesis was done using the precursors Li_2CO_3 and TiO_2 [39].

2.2 Nanocellulose Production

2.2.1 CNC

CNC starts off as alpha cellulose powder at varying weights and sulfuric acid amounts to test the best possible results [40]. The cellulose powder was placed into a glass beaker with the sulfuric acid and magnetically stirred at 200 RPM on a hot plate for 30 min, some with heat, other samples at room temperature. After the reaction is completed, the solution is diluted using

approx. 400 mL of refrigerated DI water. Then it undergoes a secondary dilution with another 500 mL of cold DI water in a 2L glass beaker. The acid bath solution is then vacuum filtered using 2.5 micron paper filters. Waste is disposed of appropriately.

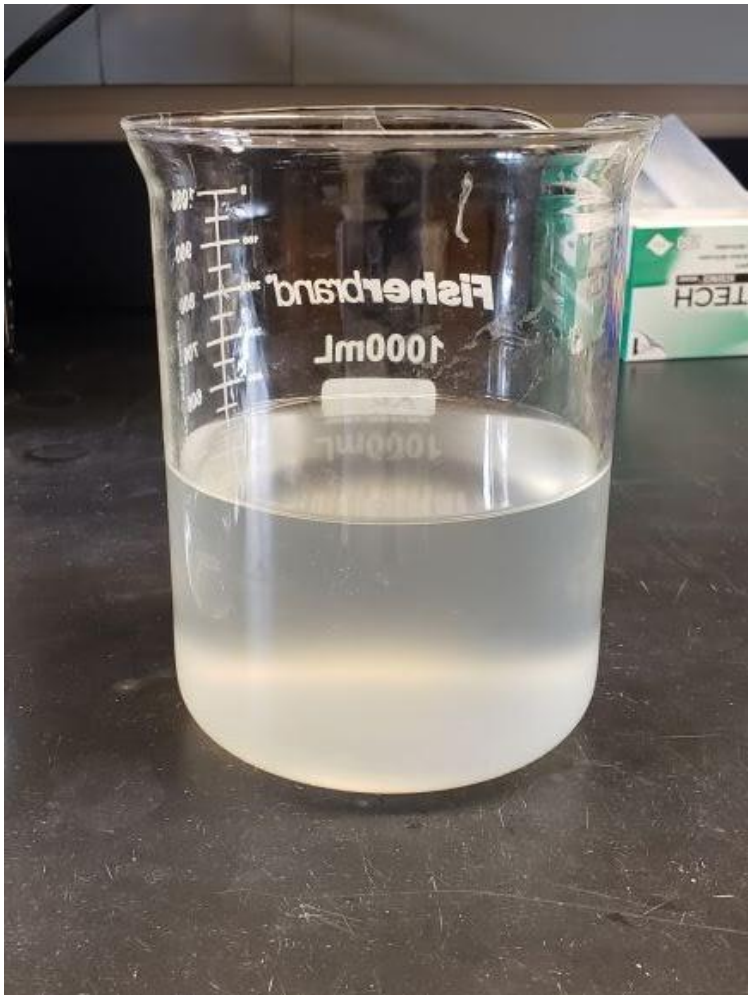

Figure 9. CNC after acid hydrolysis and dilution with DI water.

2.2.2 CNF

3g of softwood card stock was submerged in 300 mL of DI water overnight. Then the soaked pulp is magnetically stirred at 200 RPM on a hotplate for approx. 15 min to aggregate the fibers in preparation for TEMPO. As the pulp is continually stirred throughout the process, 0.3 g of solid NaBr. in a separate test tube, 0.048 g of TEMPO is dissolved in 5 mL of DI water before being added to the pulp solution. 16.447 mL of 15 mmol NaClO is added to the solution after TEMPO. Throughout the entire reaction, the solution must maintain a pH of 10; a pH probe is used to monitor the pH. 1M NaOH is added dropwise to the solution as the solution pH will naturally drop. The reaction will be done in approx. 4 hours and when the pH remains around 10 without the addition of NaOH. In addition the solution will turn from yellow to white. 1M HCl is added drop wise until the pH is neutralized to 7. The solutions are then dispersed equally in centrifuged tubes and centrifuged at 5000 RPM for 10 min. The precipitate is saved and liquid is decanted for disposal. Then dialysis bags are filled with the precipitate and submerged in a bucket filled with DI water until the conductivity is approx. 1 μS. Water is to be changed daily. Afterwards, the dialysis are cut open and emptied into a large beaker then topped to 1 L with DI water. With approx. 500 mL of the solution at a time, a house blender is used to liquefy the solution for 30 min. Then the liquified solution is sonicated at 100% amplitude for 2 min in plastic beakers. The solution is then centrifuged again at 5000 RPM for 15 min before saving the liquid and disposing the precipitate [41].

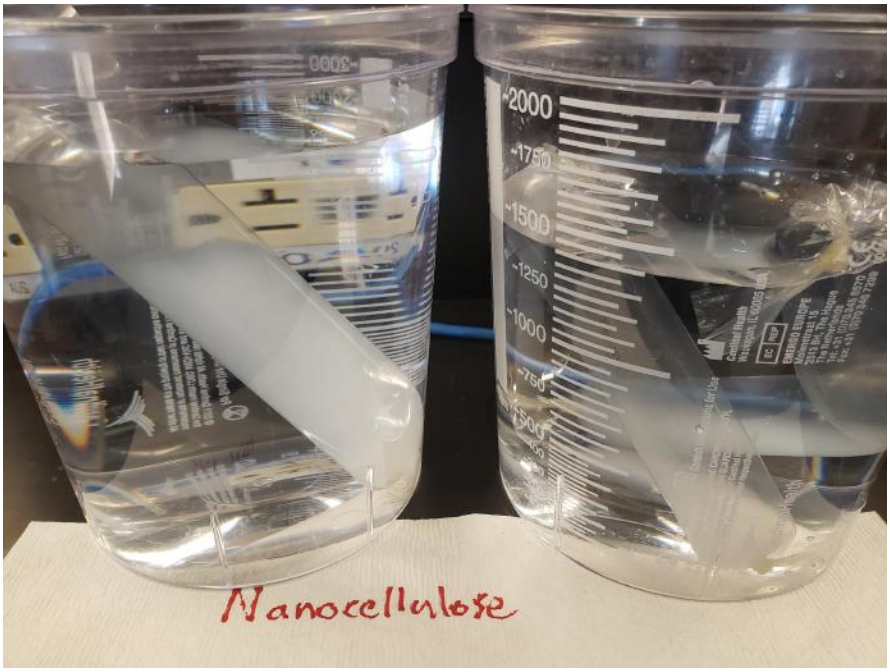

Figure 10. CNF after TEMPO oxidation, in dialysis bags submerged in DI water to wash away excess chemicals used during the oxidation process.

Figure 11. CNF after washing and mechanical defibrillation with a house blender.

2.2.3 BC

The BC was obtained from colleagues that they grew and harvested themselves. According to their procedure, the BC started off as a SCOBY starter kit that was fermented in a large fish tank for 3-4 weeks before being harvested [42]. The harvesting procedure is as follows, "Bacterial cellulose was harvested as a sheet from the tank and immersed in 1 liter of 1 mol/L sodium hydroxide solution. The solution was kept stirring at 90°C for 1 hr at 150 RPM. Air cooling the solution was followed by progressive dilution with deionized water till a neutral pH was achieved. The cellulose sheet was washed by rinsing in a beaker with deionized water for 2 times followed by 24 hours deionized water soaking and repeat the rinsing and soaking process for about 7 times or until the pH of the solution reaches 7 and the color of the pellicle turn from brown to white."

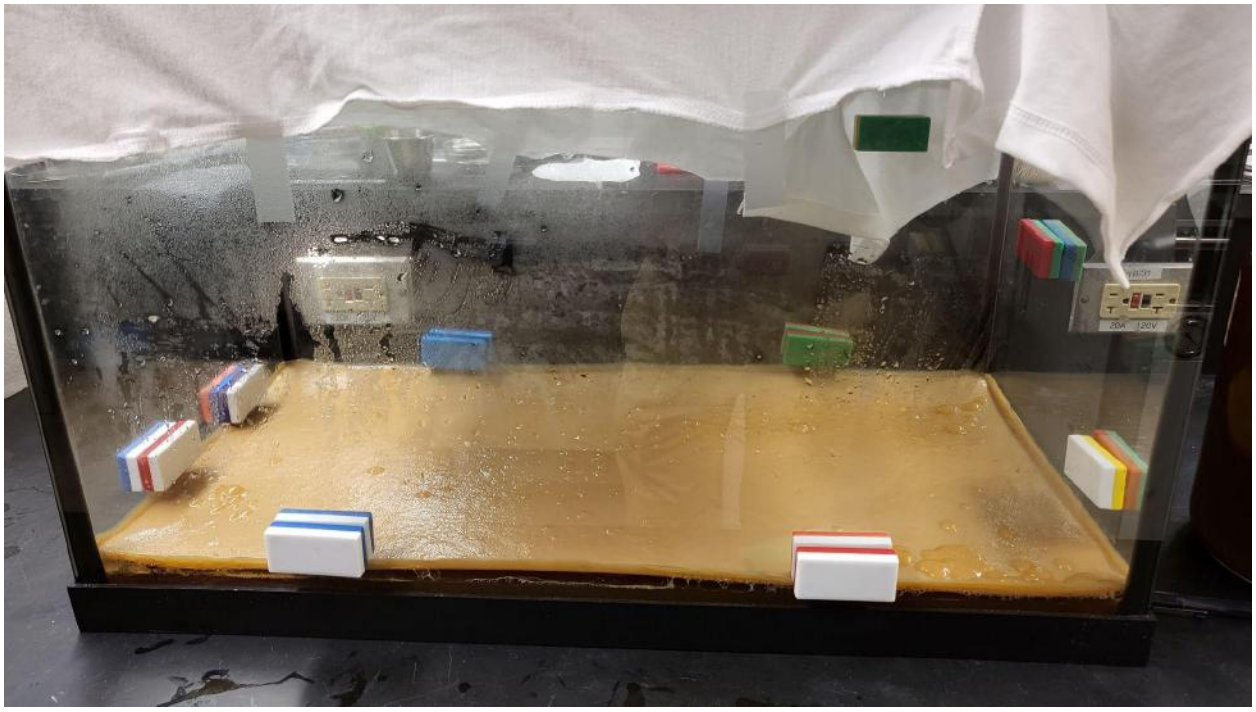

Figure 12. Bacterial cellulose growing in the lab.

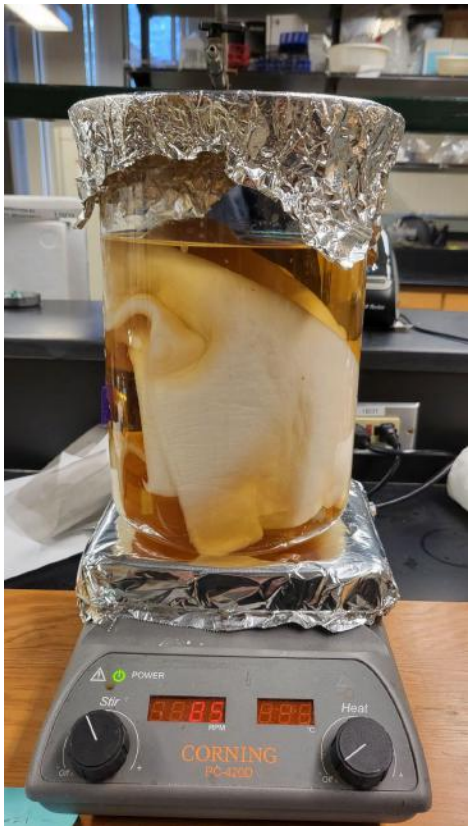

Figure 13. Bacterial cellulose harvested from the fish tank and currently being cleaned with DI water after it was bathed with sodium hydroxide.

2.3 Preparation of HTO

Li_2CO_3 and TiO_2 powder precursors were first mixed together at the appropriate molar ratios (15g, Ti 0.187 mole and 13.9g 0.376 Li) respectively, and ground in an agate mortar for 20-30 min. Then the powder is placed in an alumina crucible and heated in an oven at a rate of 6 °C/min up to 700°C for 4 hours. Once the powder is completely cooled, it is ground and sieved to produce Li_2TiO_3. In order to convert Li_2TiO_3 into H_2TiO_3, 1g of Li_2TiO_3 per 1L of 0.5 HCl is placed on a hotplate and magnetically stirred for approx. 2 days. It is then centrifuged in 50 mL tubes for 10 mins at 8000 RPM and washed 3 times with DI water. The washed powder is finally dried overnight in an oven at 60 °C to obtain fully converted HTO powder [39].

2.4 Preparation of Metal Nitrates

Metal nitrate solutions were made using solid $Ca(NO_3)_3$, $Zn(NO_3)_3$, and $Cu(NO_3)_3$ pellets and mixing with the required amounts of DI water. Each solution was made to 0.05M to a final volume of 800 mL. 3 1000 mL glass bottles were filled with 9.446g, 11.899g, and 9.664g of $Ca(NO_3)_3$, $Zn(NO_3)_3$, and $Cu(NO_3)_3$ pellets, respectively, and topped off to 800 mL with DI water. Then they were mixed vigorously until they were all a homogenous solution [43]. Before use, the solutions were shaken to aggregate particles.

2.5 Fabrication of Hydrogel

Several different types of cellulose were tested to make a robust, self-standing hydrogel. The first was using hydroxyethyl cellulose. Equal parts hydroxyethyl cellulose powder and metal nitrate solution was added into a 50 mL test tube with 20 mL of DI water. Each tube was stirred vigorously before allowing it to react for approx. 24 hours. CNC and CNF hydrogels were also attempted to be produced in a similar way. Approx. 20 mL of each respective nanocellulose solution were added to 50 mL test tubes along with equal volume metal nitrate solutions, with and without mixing, and left to react for 24 hours. Another batch of CNF hydrogels were also produced using more concentrated CNF (approx. 12%) with the same method. The metal nitrates act as a crosslinker between the multiple fibers and should form a hydrogel if the metal nitrates crosslink properly. Freeze drying the hydrogels was also attempted to see if it would increase the robustness. The hydrogel was frozen for approx 1 day in the freezer then freeze dried.

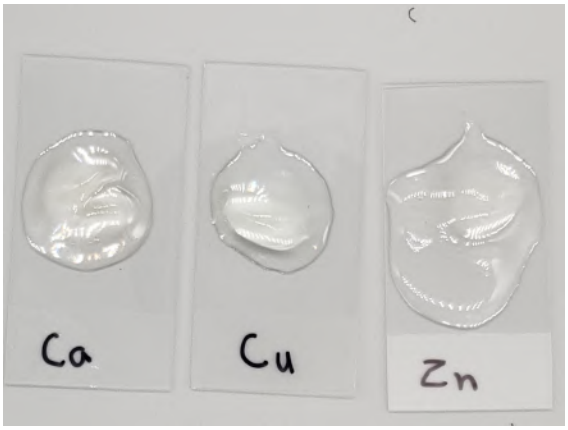

Figure 14. hydroxyethyl cellulose powder after mixing with DI water.

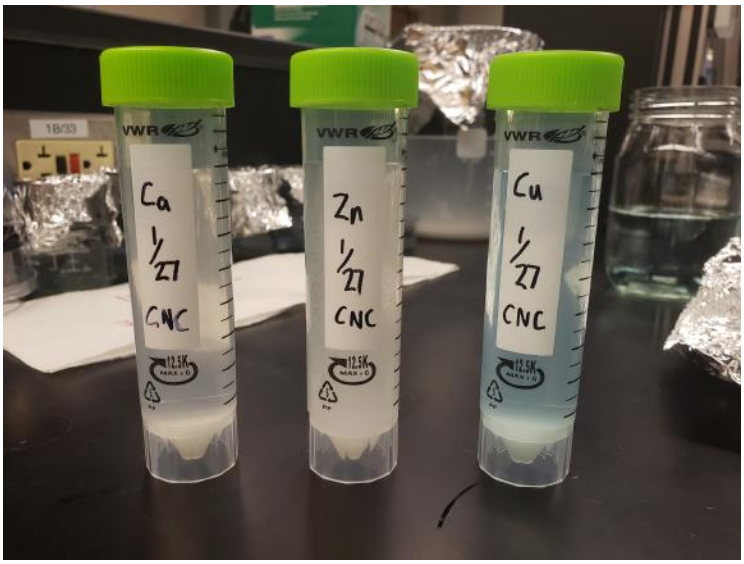

Figure 15. CNC mixed with metal nitrate solutions, note that the CNC sunk to the bottom of the test tube meaning it is not cross linking properly.

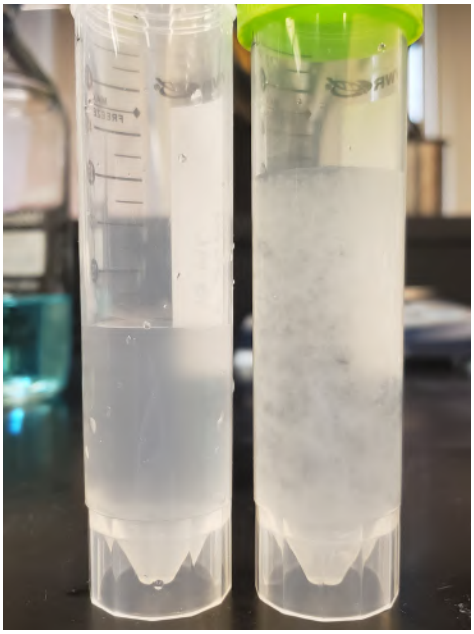

Figure 16. (Left) a test tube with just CNF. (Right) a test tube of CNF mixed with metal nitrate solution. Note that it is cross linking but not enough to form a proper hydrogel.

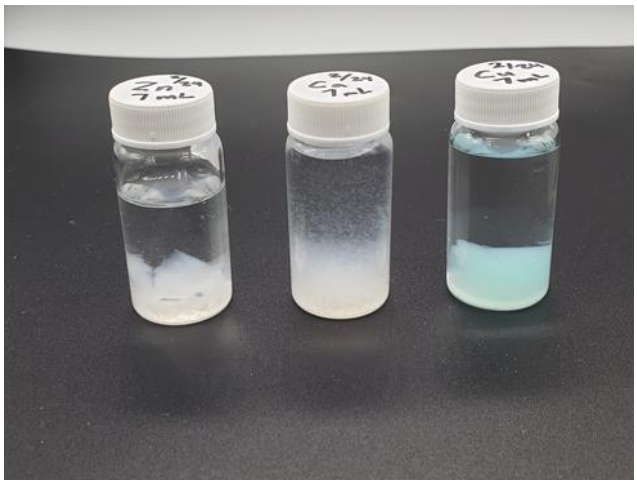

Figure 17. Small vials of CNF mixed with metal nitrate solutions. From left to right, CNF is mixed with $Zn(NO_3)_3$, $Ca(NO_3)_3$, and $Cu(NO_3)_3$. Note that a hydrogel is now forming.

2.6 Fabrication of BC Composites

2.6.1 Hydrogel

HTO particles with 10 mL of DI water were either aggregated in a sonication bath for 24 hours or ultrasonicated with a probe at 25% amplitude for 5 min. Pure BC pellicles were cut down to 2.5 cm x 2.5 cm pieces. Two infiltration methods were tested on the hydrogel; a passive and active method. The BC pellicles were put into a 40 mL test tube with 0.01g of HTO mixed with 10 mL of DI water and bath sonicated for 24 hours as passive infiltration [44]. For active infiltration, a funnel, vacuum pump and a filter flask was used [45]. In order to gain a better seal, a piece of 20 micron filter paper was placed between the BC pellicle and the funnel. Each pellicle was vacuum filtered at a specified time, after each cycle the pellicle was flipped over to ensure equal distribution of both sides and the process was repeated.

Table 2. Overview of different methods tested on BC pellicles for optimal HTO infiltration.

Sample	NP Concentration (g/mL)	NP Solution Volume (mL)	NP Mixing Method	Infiltration Method	# of Passes/Time
1	0.001	10	Sonication Bath	Vacuum	10
2	0.001	10	Ultrasonic Probe	Vacuum	10
3	0.001	10	Sonication Bath	Sonication Bath	24h

2.6.2 Aerogel (Freeze-Dried)

Before active infiltration for the aerogel, the BC pellicles were first frozen in the refrigerator for 24 hours until completely frozen or frozen using liquid nitrogen. Then they are placed into a freeze-dryer (Freezone 2.5L, Labconco Corporation, Kansas city, MO) at approx -50℃ and 0.036 mBar for 24-36 hours or until fully dried [46]. The same procedure for vacuum filtration as the hydrogels were done on the aerogels. The nanoparticles were ultrasonicated at 25% amplitude for 5 minutes before vacuum infiltration twice, flipping between each cycle. The infiltrated aerogels are then air dried at room temperature for 24 hours.

Table 3. Overview of Nanoparticle mixing method and infiltration method on freeze-dried BC.

NP Mixing Method	Infiltration Method	# of Passes/Time
Ultrasonic Probe	Vacuum filter	2

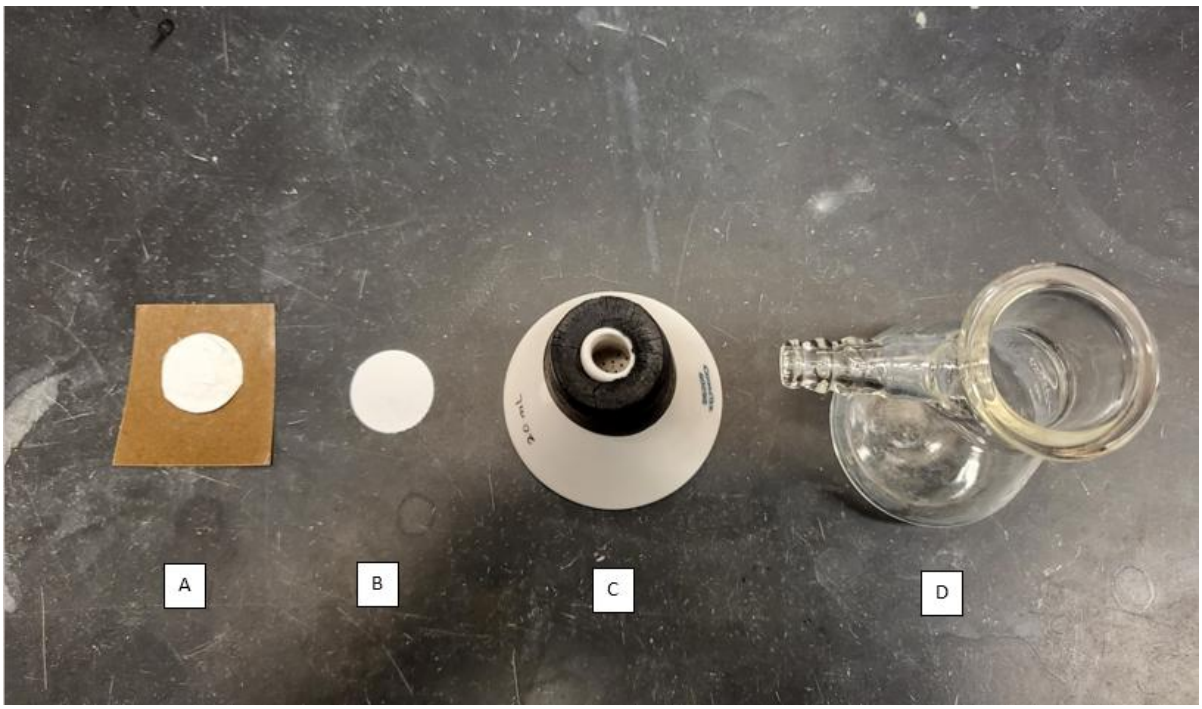

Figure 18. An overview of the vacuum infiltration setup, (A) cut piece of freeze-dried BC, (B) cut piece of 2.5 micron filter paper, (C) ceramic filter funnel, (D) 125 mL vacuum flask.

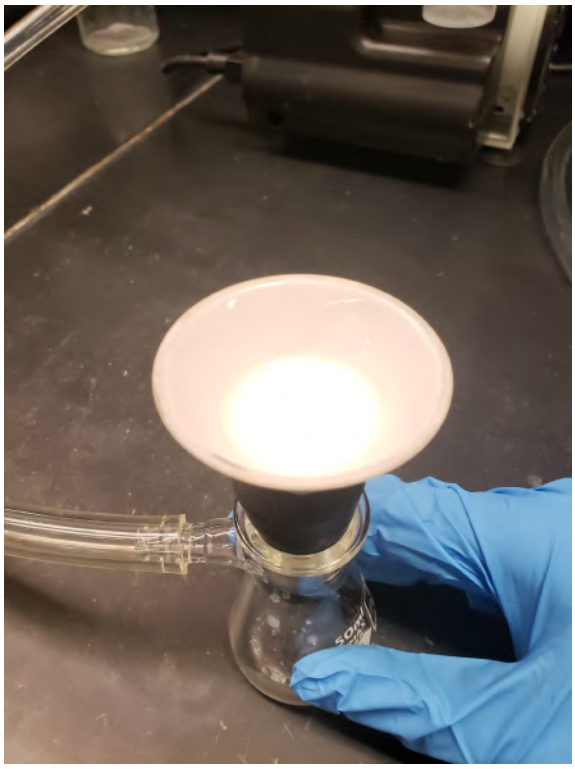

Figure 19. Freeze-dried BC being vacuum filtered with ultrasonication probed HTO solution.

2.7 Characterization Methods and Analysis

2.7.1 SEM

"The samples were coated with 5 nm of platinum in a Leica EM ACE600 sputter coater. SEM Imaging was conducted in a ThermoFisher Scientific Apreo variable-pressure SEM at an accelerating voltage of 10 kV. The images were acquired in a mixed BSE/SE (50%/50%) mode."

2.7.2 TGA

"TGA measurements were conducted in a D550 TGA from TA Instruments, (New Castle, DE). Samples were heated from room temperature to 1000°C at a heating rate of 1°C/min in air flow at 40 mL/min."

Chapter 3 – Results and Discussion

3.1 Picking a Proper Cellulose Scaffold

3.1.1 Structural Properties

CNC was unsuccessfully produced using the desired method and conditions. Instead of obtaining a homogenous solution with nanocellulose particles, a variety of different products were created. All were reacted under similar conditions with some variation in acid amount and cellulose amount. Using heat, the acid bath solution was burned into the black gel-like substance. Without heat, the solution turned into a tan colored viscous gel that was then vacuum filtered, dried and turned into white, malleable solids. Looking under an optical microscope, it also does not appear that the morphology of the cellulose powder did not change to the desired composition. However CNC was not the main focus of this project, it was only an alternative and to see if CNC could be produced under our conditions.

Table 4. Overview of different CNC acid hydrolysis conditions.

Batch #	Cellulose (g)	H2SO4 (mL)	RPM	Time (min)	Temp (C)	1st Dilution (mL)	2nd Dilution (mL)
1	5	10	220	30	NA	400	500
2	5	15	150	30	NA	400	500
3	15	15	200	30	NA	400	600
4	15	35	200	30	NA	400	NA
5	15	35	200	30	49	NA	NA
6	15	22.5	220	30	46	400	NA

Figure 20. Alpha cellulose powder during acid hydrolysis with sulfuric acid.

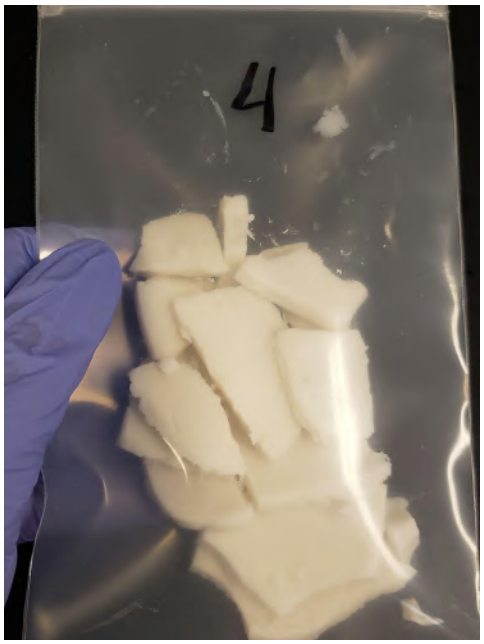

Figure 21. Malleable solids obtained after vacuum filtering solution from acid hydrolysis.

Figure 22. Black substance from acid hydrolysis.

Standard alpha cellulose powder was also mixed with the metal nitrate solutions to see if it would react to form a gel. The cellulose powder did not react at all with the solution, with and without agitation after leaving it overnight. A gel was successfully made using hydroxyethyl cellulose and metal nitrate solutions. However the gel was not stable in water and even out of water, it loses its viscosity after several days. Even with more cellulose powder, the gel was not robust enough for this certain application. A mixture of containers were also used to see if there was a noticeable difference in stability. The gels made using the hydroxyethyl cellulose were also freeze-dried in an attempt to make aerogels. Aerogels were made however they easily disintegrated once it was put into water.

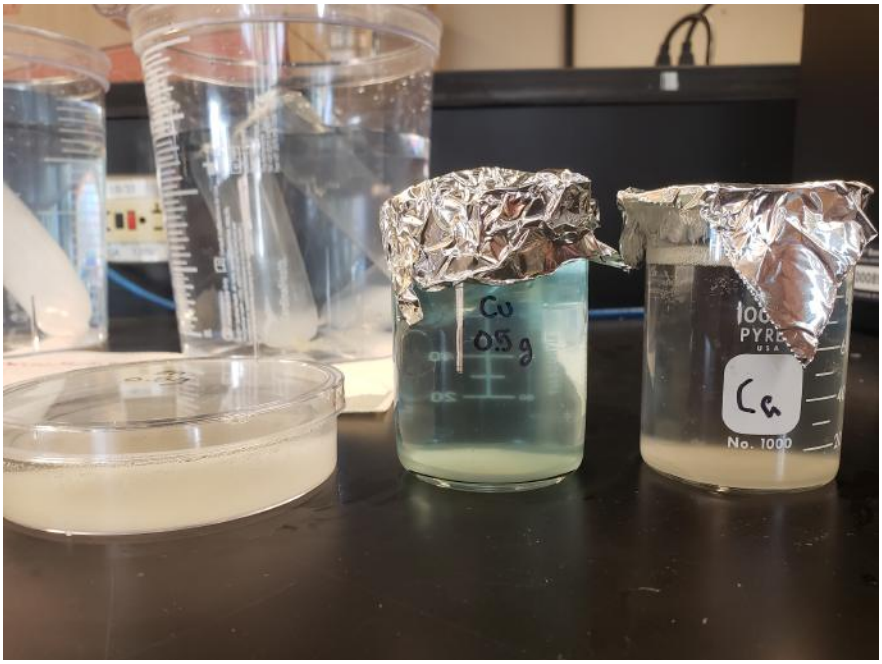

Figure 23. Alpha cellulose powder mixed with metal nitrate solution.

Table 5. Overview of different hydrogel mixing conditions with hydroxyethyl cellulose.

Batch	Cellulose Type	Cellulose (g)	Water (mL)	Containers	Cu (mL)	Ca (mL)	Zn (mL)	Gel Formation
1	Hydroxyethyl Cellulose	0.2	20	Test Tubes	16.55	16.94	13.44	Yes
2	Hydroxyethyl Cellulose	0.3	20	Petri Dish	24.83	25.41	20.17	No
3	Hydroxyethyl Cellulose	0.5	50	Beaker (Cu, Ca) + Petri Dish (Zn)	50	50	50	Only in Beakers
4	Hydroxyethyl Cellulose	0.3	30	Test Tubes	24.83	25.41	20.17	Yes
5	Hydroxyethyl Cellulose	0.75	30	Beaker	62.09	63.52	50.42	Yes

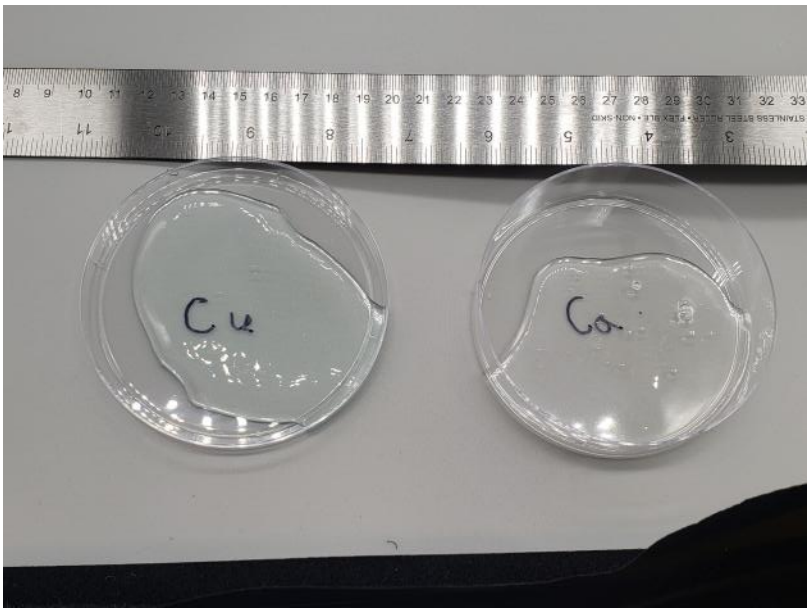

Figure 24. Hydroxyethyl cellulose mixed with (Left) $Cu(NO_3)_3$ solution and (Right) $Ca(NO_3)_3$ Solution in petri dishes.

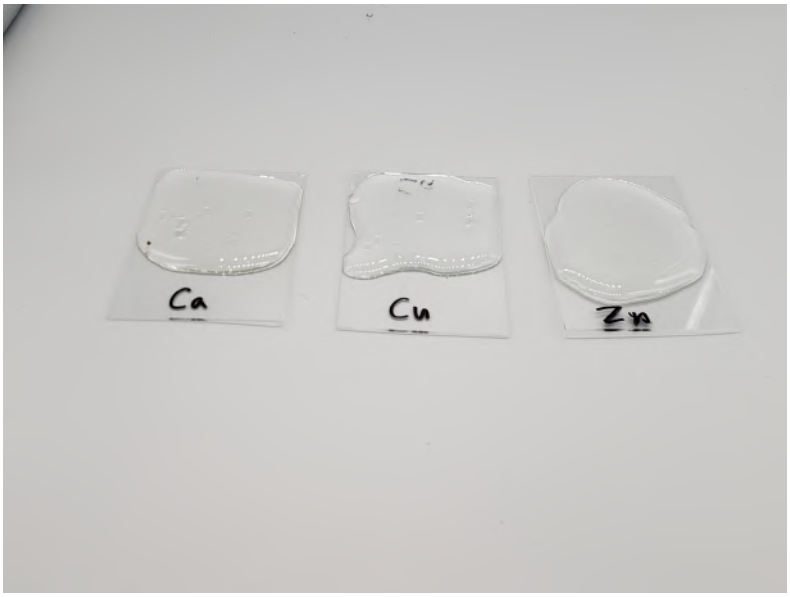

Figure 25. Hydroxyethyl cellulose mixed with $Ca(NO_3)_3$, $Cu(NO_3)_3$and $Ca(NO_3)_3$ solution placed on microscope slides.

Figure 26**.** Hydroxyethyl cellulose hydrogel frozen in freezer then freeze dried.

CNF was produced successfully using a combination of TEMPO oxidation and mechanical defibrillation. However there are some flaws with the CNF, specifically impurities due to no centrifugation done on the batch. Regardless though, the first batch of CNF was made successfully and a somewhat robust hydrogel was made using the metal nitrates. In an attempt to increase the durability of the gel, a second batch of CNF was produced. This time more concentrated in weight by volume and also doubling the amount of NaClO added and increasing it to 25 mmol per g of fiber during the reaction in order to increase oxidation and fiber to fiber interactions [47]. With these two modifications, a robust hydrogel was synthesized. It was stable in water for long periods of time and maintained its shape very well even under minor pressure or agitation. But as a platform for HTO infiltration, it was not the right solution. With enough agitation, it still broke apart too easily for this project.

Figure 27. Side view of $Cu(NO_3)_3$ solution added to CNF. Note that the cross linkers are partially working and forming something in the solution.

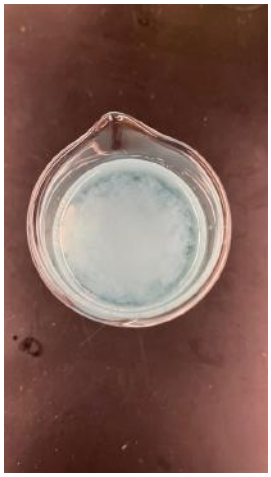

Figure 28. Top view of $Cu(NO_3)_3$ solution added to CNF.

Figure 29. CNF hydrogel created after adding $Cu(NO_3)_3$ and waiting for 24 hours to completely react. Note that the solution was not agitated or mixed for hydrogel to form.

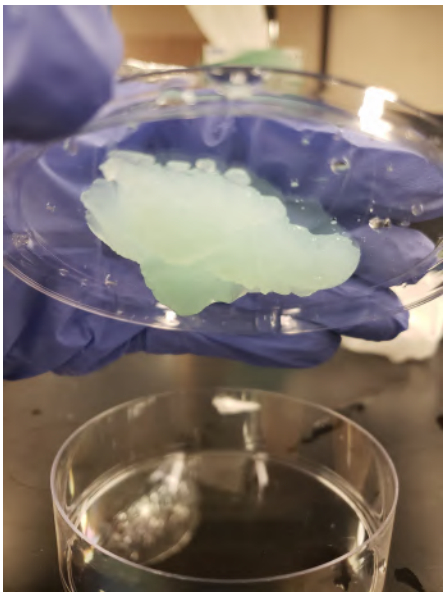

Figure 30. Demonstrating the stability of the hydrogel, it does not fall apart under gravity.

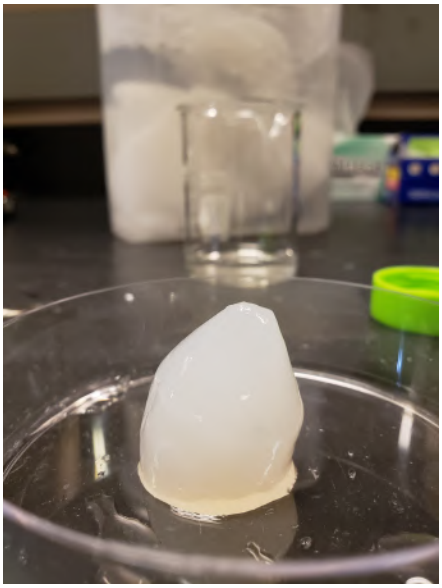

Figure 31. CNF/$Cu(NO_3)_3$ hydrogel.

BC was successfully cultivated into large sheets 16” x 8”, cleaned, and cut down into smaller pieces for ease of use. In its original form as a hydrogel pellicle, BC was very stable and robust, lending its properties to the network of interconnected nanocellulose fibers with strong hydrogen bonds and Van Deer Waals interactions. Pulling on the pellicles by hand and submerging in water did not affect its macrostructure. SEM images, analyzed using ImageJ, show that the average diameter of the BC was 56 nm, with a standard deviation of 16.5 nm based on 2 images (BC40 and BC41) and 50 measurements taken from each image. This makes BC pellicles an ideal candidate as the cellulose scaffold for HTO infiltration due to its robust and stable nature.

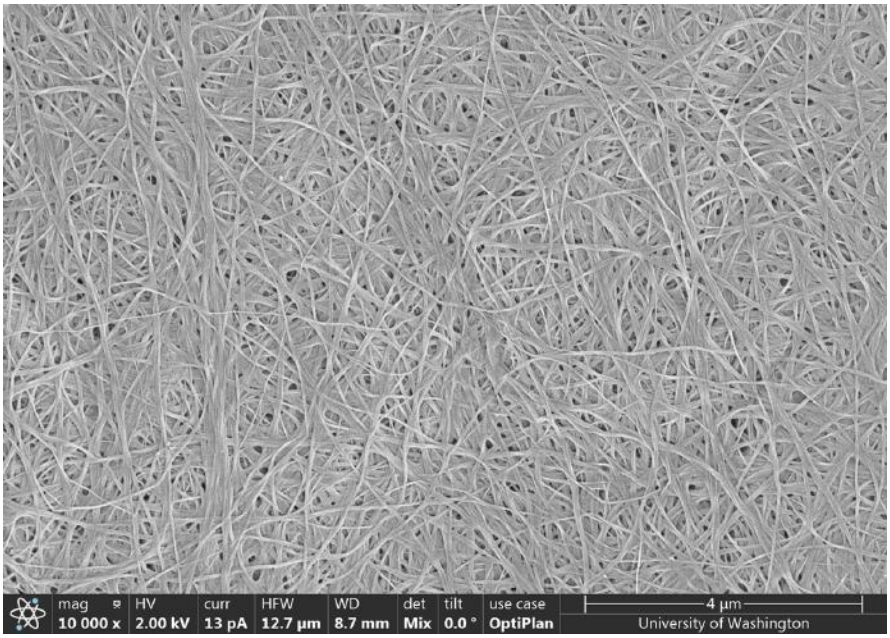

Figure 32. (BC40) SEM images of BC pellicles showing the individual nanofibers.

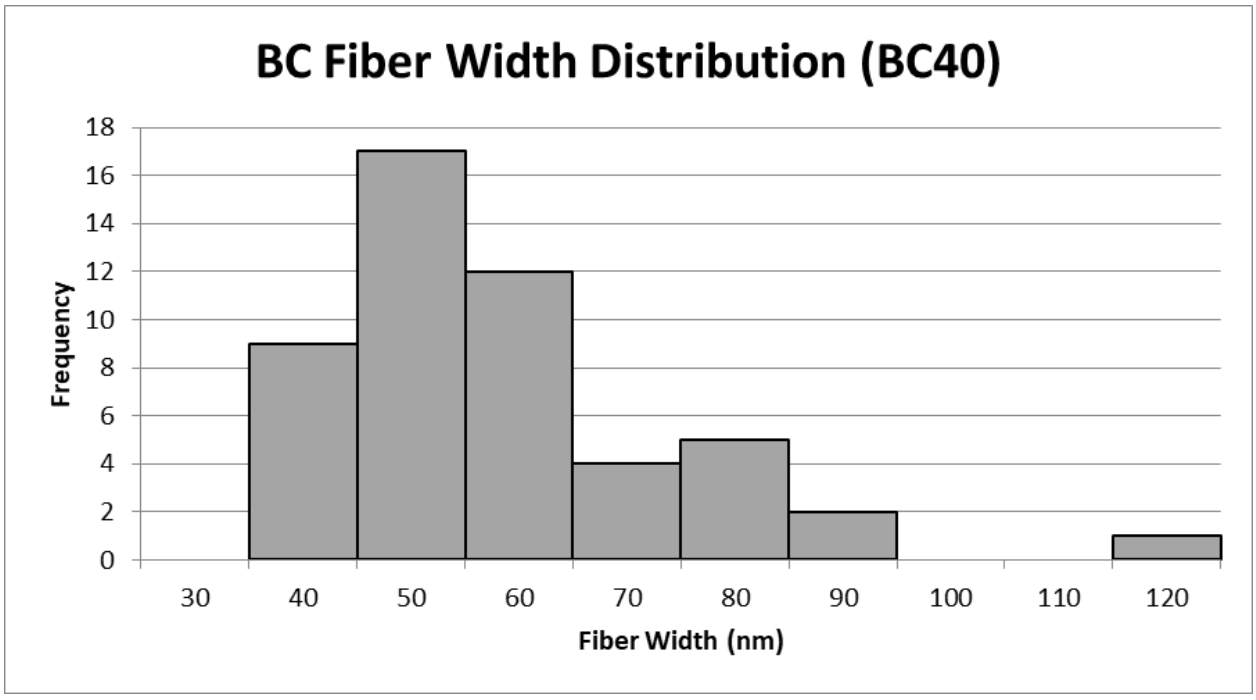

Figure 33. BC fiber width distribution based on 50 measurements taken from image BC40.

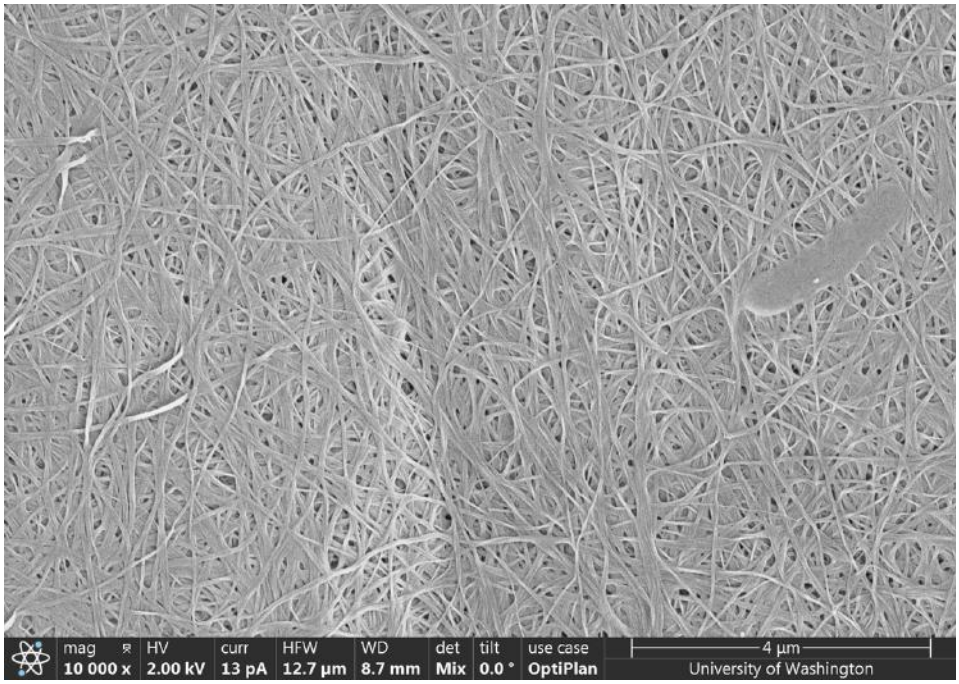

Figure 34. (BC41) SEM images of BC pellicles showing the individual nanofibers.

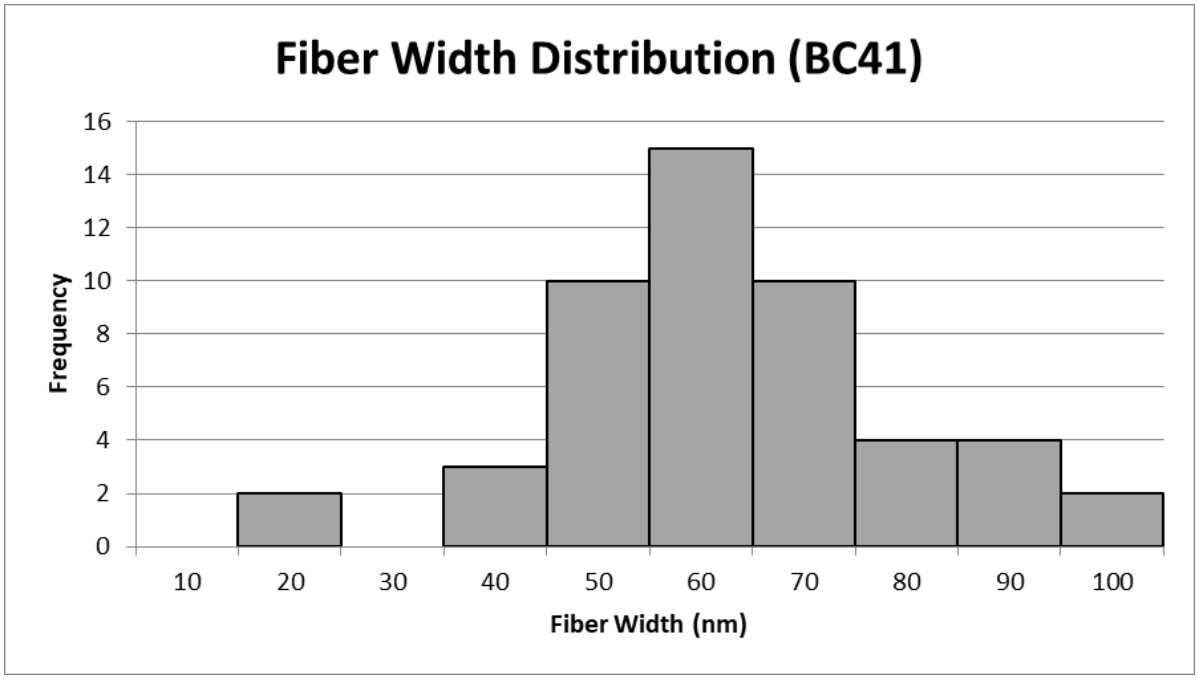

Figure 35. BC fiber width distribution based on 50 measurements taken from image BC41.

3.1.2 Acid Stability Test

An additional stability test is done on the CNF hydrogel and BC pellicle to determine if they would maintain their structure in HCl. approx 1 g of each cellulose scaffold was submerged in 100 mL of 0.2M HCl for 24 hours to see the effects. This is important since one of the factors is reusability and the scaffolds will have to be submerged into HCl to harvest the Li ions captured within the scaffolds. After 24 hours, both the scaffolds appear to remain intact and largely unaffected by the HCl. However, the BC pellicle remained the most suitable candidate due to its more robust nature and thus future testing and experiments will be done with the BC.

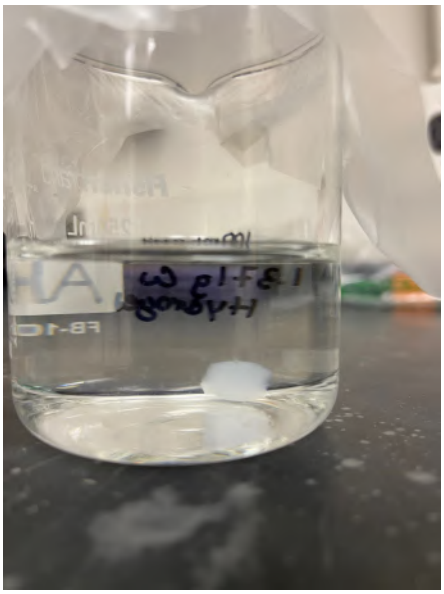

Figure 36. A piece of CNF hydrogel submerged in 100 mL of 0.2M HCl.

Figure 37. A piece of CNF hydrogel submerged in 100 mL of 0.2M HCl. 1 week later.

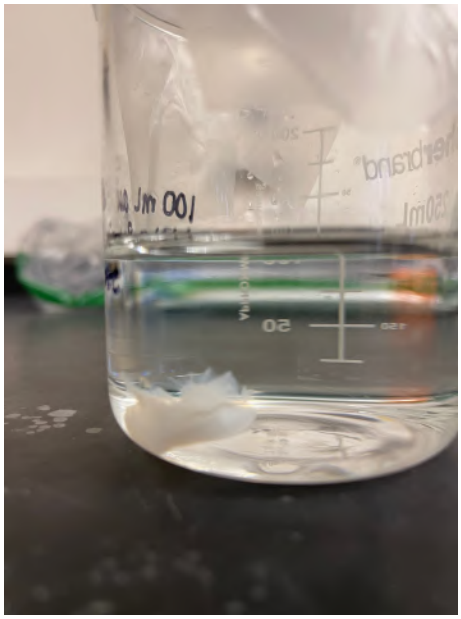

Figure 38. A piece of BC hydrogel submerged in 100 mL of 0.2M HCl.

Figure 39. A piece of BC hydrogel submerged in 100 mL of 0.2M HCl. 1 week later.

3.2 HTO Particle Size Distribution

HTO particle size distribution was analyzed using SEM and ImageJ. Average diameter of the HTO particle was 95 nm with a standard deviation of 54 nm based on 50 measurements taken from the image below.

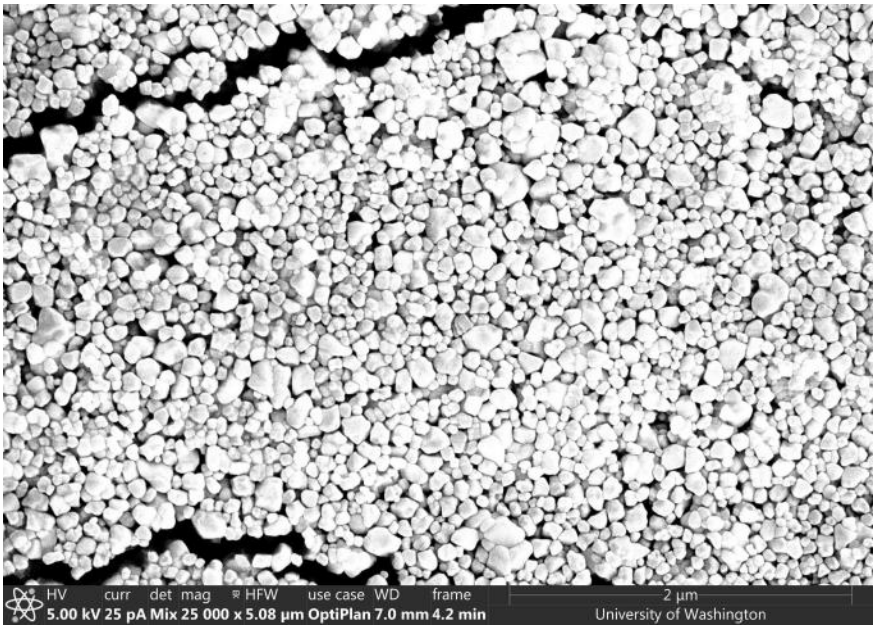

Figure 40. SEM image of HTO nanoparticles.

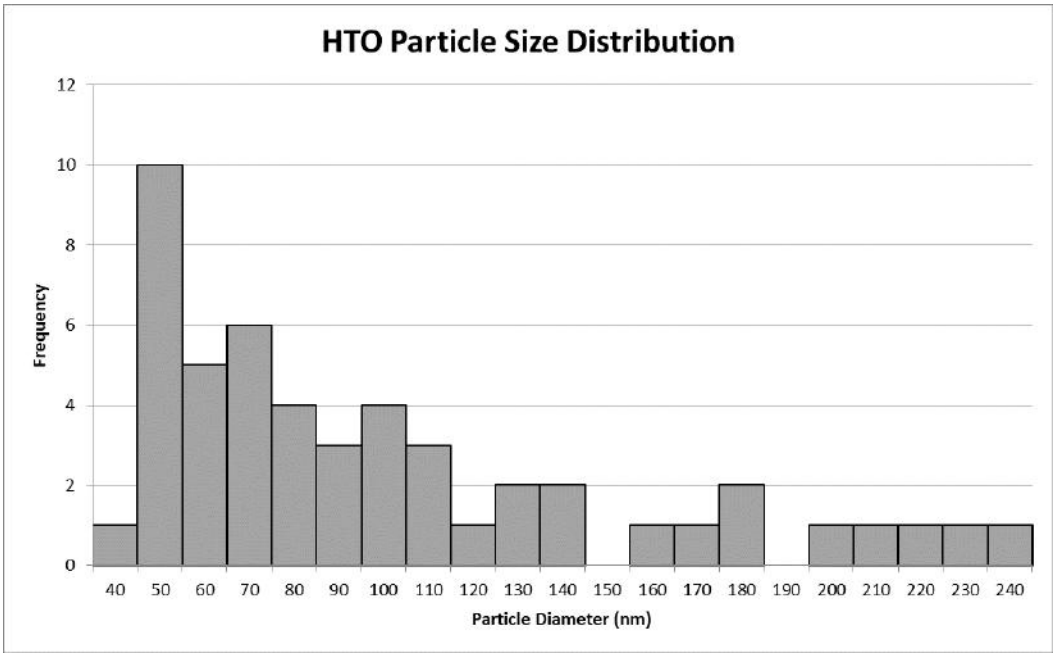

Figure 41. HTO nanoparticle diameter distribution based on 50 measurements taken from Figure 40.

3.3 Evaluation of BC Hydrogel vs BC Aerogel

The next step is to determine which BC form will be the most appropriate: hydrogel or aerogel. One of the main reasons to test this is the porosity of each structure which will affect the particle infiltration process. In theory, freeze-dried BC should be more porous due to the water in the structure compared to the hydrogel and should intake the HTO better. This will be based on: effectiveness of particle infiltration and HTO particle retention.

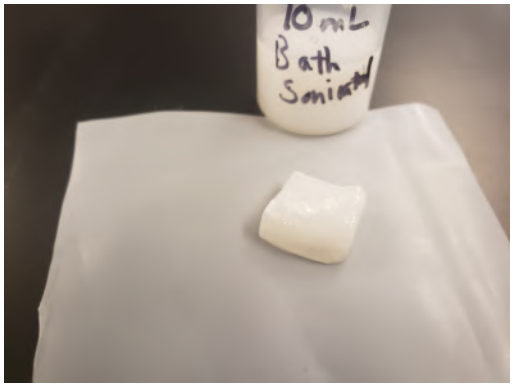

Figure 42. Piece of BC hydrogel after infiltrating with HTO via bath sonication.

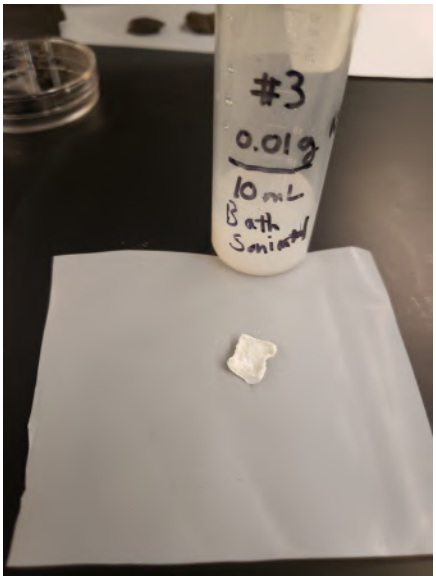

Figure 43. Piece of BC hydrogel after infiltrating with HTO via bath sonication and air dried for 24 hours.

Effectiveness of particle infiltration is determined by how well the BC is able to intake the HTO particles into their porous structure. This will then be compared via SEM images. These SEM images represent the HTO particles within the BC microstructure. The first image is of the hydrogel and it may seem like the HTO was successfully infiltrated but upon closer inspection, this was on the surface and not many of the HTO particles actually made it to the inner layers.

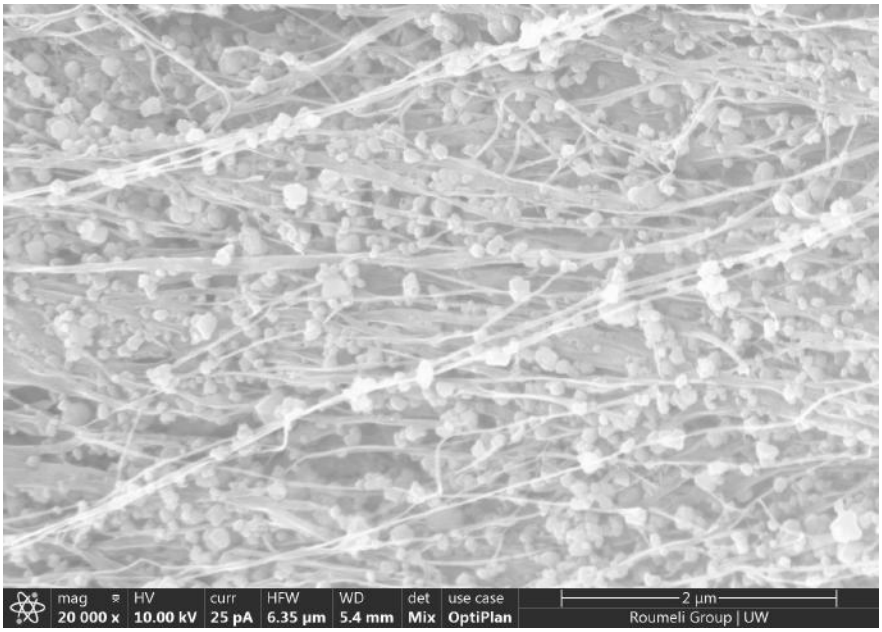

Figure 44. SEM images of BC hydrogel infiltrated with HTO particles using vacuum infiltration after air drying. Note that most of the particles remained on the surface of the hydrogel.

This set of images represent the aerogels and compared to the hydrogels, the particles actually made it closer to the inner layers meaning there is a better distribution of the HTO throughout the entire pellicle itself.

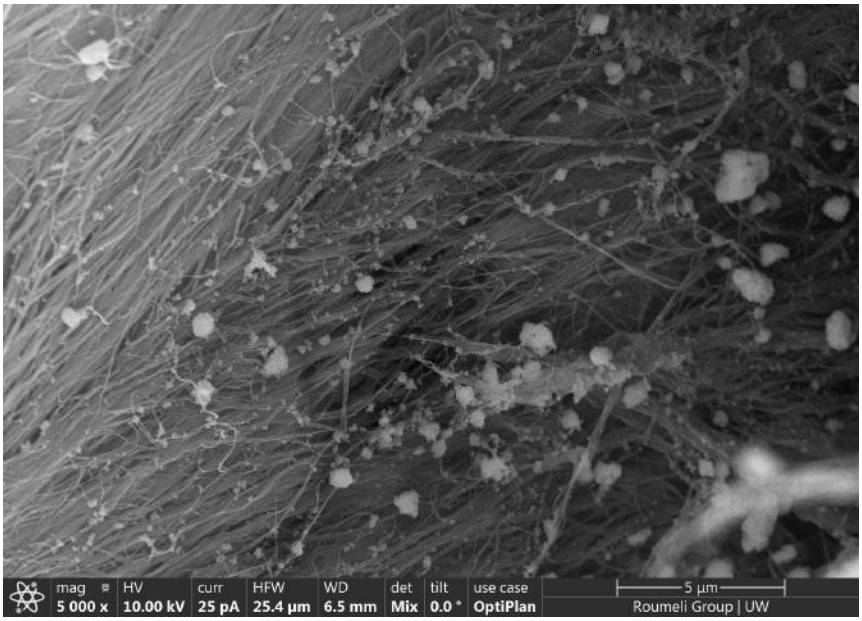

Figure 45. SEM images of BC aerogel infiltrated with HTO particles using vacuum infiltration after air drying. Note that the particles made it throughout the structure unlike the hydrogel.

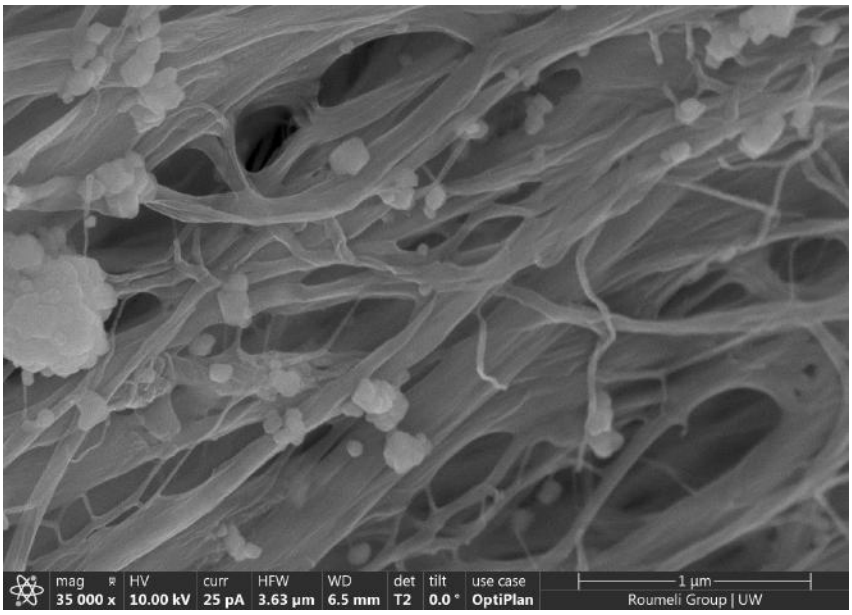

Figure 46. SEM images of BC aerogel infiltrated with HTO particles using vacuum infiltration after air drying. Closer look into the structure.

3.3.1 Cycling Test

HTO particle retention is tested via a cycling test with DI water and 0.2M HCl. Both the hydrogel and aerogel were vacuum filtrated with approx. 0.01g of HTO in 10 mL of DI water. Before cycling, each type of composite is first tested on the TGA to get a baseline on HTO wt %. Then the pellicles are swapped between the water and HCl 6 total times with 12 hours between each swap for a total of 3 days. After being air dried, each pellicle is then tested on the TGA to see the change in wt % before and after cycling. This would confirm the amount of HTO that was infiltrated into the composite initially and the amount lost after testing.

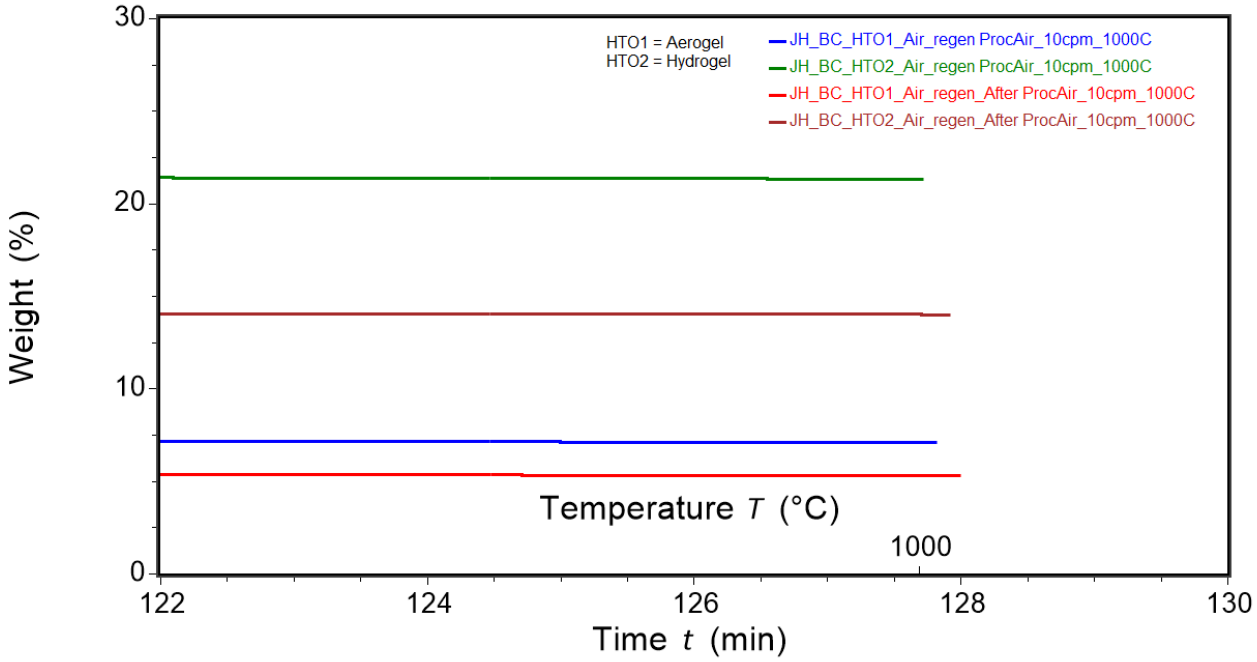

Figure 47. TGA graph showing the weight % of HTO left in the BC aerogel composite vs BC hydrogel composite after pyrolysis. Both infiltrated using vacuum filtration.

Table 6. Results of TGA testing after cycling test for aerogel and hydrogel.

Samples	Before	After	Wt. % Lost	Wt. % Change
Aerogel	7.093	5.313	1.78	25.095
Hydrogel	21.339	14.019	7.32	34.303
Aerogel (2)	7.093	4.755	2.34	32.990
Hydrogel (2)	21.339	13.835	7.50	35.147

Each piece was tested twice for consistency purposes. Overall, the HTO wt% lost was greater in the hydrogel even though the hydrogel had more HTO in it. This also confirms the SEM images that the HTO was infiltrated more successfully in the aerogel than the hydrogels. One possible reason the hydrogel lost more HTO is because the particles themselves remained mostly on the

surface. After doing the acid stability and cycling test, freeze-dried BC or BC aerogel was chosen as the primary cellulose scaffold due to it being able to intake HTO particles better and deeper into the scaffold and its ability to retain those particles more effectively after multiple washing cycles.

3.4 BC Composite Fabrication Analysis

Testing was done on both the hydrogel and aerogel to determine whether passive or active infiltration was more effective. BC composites were tested based on the table below. 3 Samples were tested with vacuum infiltration, one being freeze-dried BC, and the other one was bath sonicated for 24 hours. TGA testing shows that, for this batch of composites, all the HTO wt % were relatively close to each other. To note, the wt% of the BC composite was subtracted with TGA testing done on pure BC wt % in order to get better results of the actual HTO wt % remaining. It was determined that using the ultrasonication probe was more effective at aggregating and dispersing the particles in the solution itself. After testing passive vs active infiltration of the BC composites, active infiltration using the vacuum filter would be best suited for future testing due to the greater force generated that would help evenly distribute the nanoparticles through the BC scaffold. To note, there was an error when measuring the weight % of Sample 2, but testing done on future batches confirm that the method used was the best suited out of the two shown.

Table 7. Overview of different conditions for HTO infiltration.

Sample	NP Concentration (g/mL)	NP Solution Volume (mL)	NP Mixing Method	Infiltration Method	# of Passes/Time
Hydrogel 1	0.001	10	Sonication Bath	Vacuum	10
Hydrogel 2	0.001	10	Ultrasonic Probe	Vacuum	10
Hydrogel 3	0.001	10	Sonication Bath	Sonication Bath	24h
Aerogel	0.001	10	Ultrasonic Probe	Vacuum	2

Table 8. Overview of TGA results comparing left over wt% of pure BC and BC composites.

Sample	Weight %	HTO Weight % (Difference of Sample with BC)
BC	1.464	NA
Hydrogel 1	8.956	7.492
Hydrogel 2	1.181	-0.284
Hydrogel 3	8.019	6.555
Aerogel	8.308	6.844

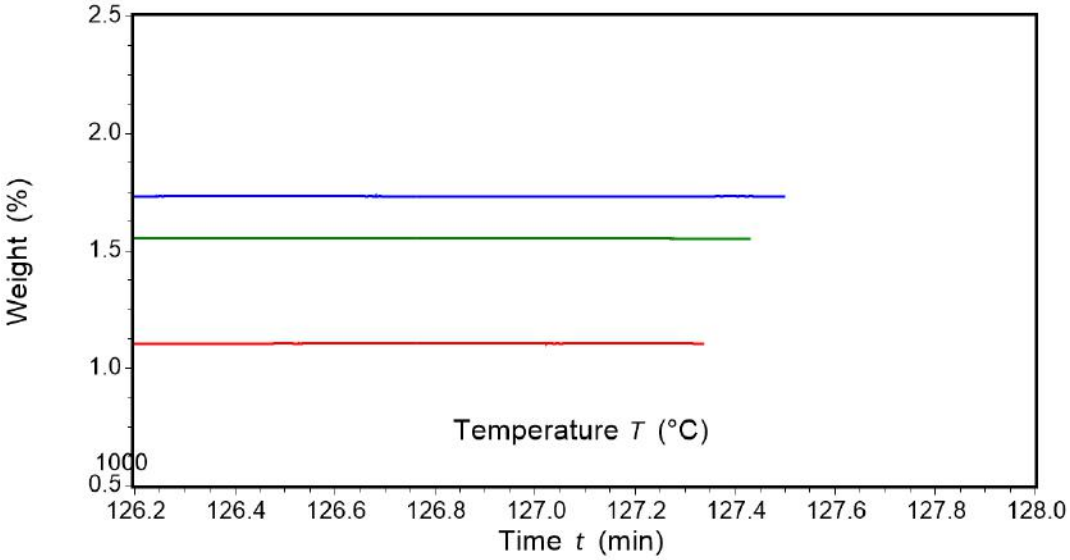

Figure 48. TGA results of pure BC, 3 different measurements with an average of 1.464 wt %.

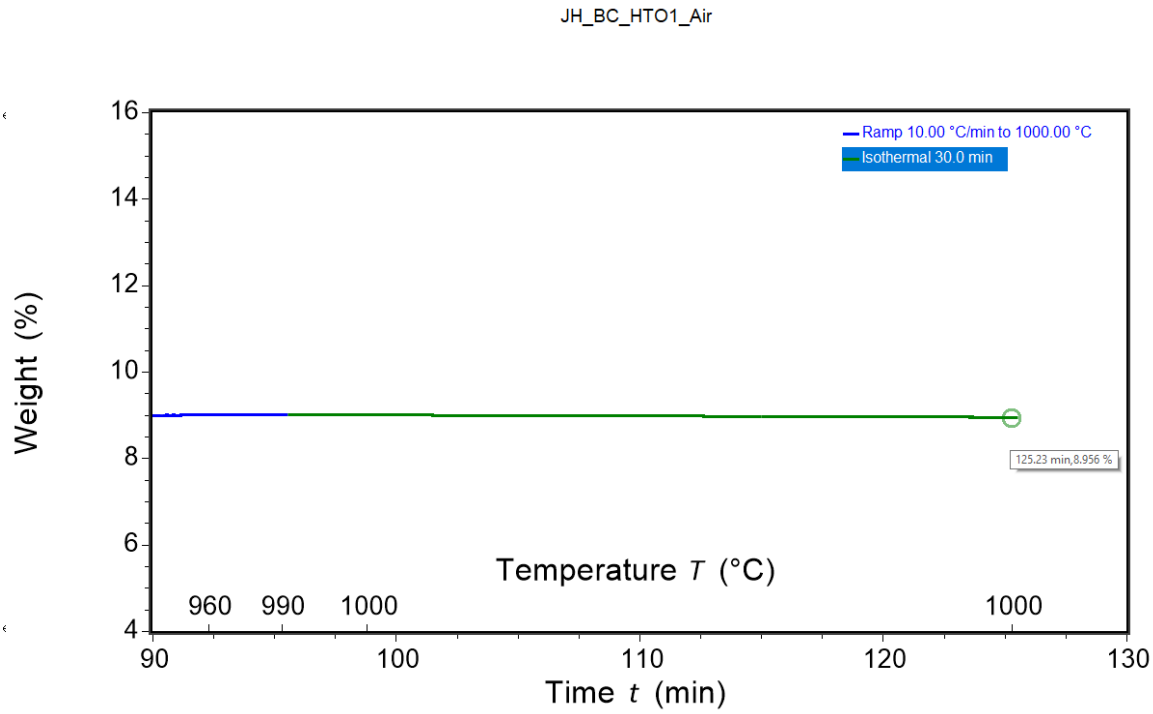

Figure 49. TGA results of Hydrogel 1.

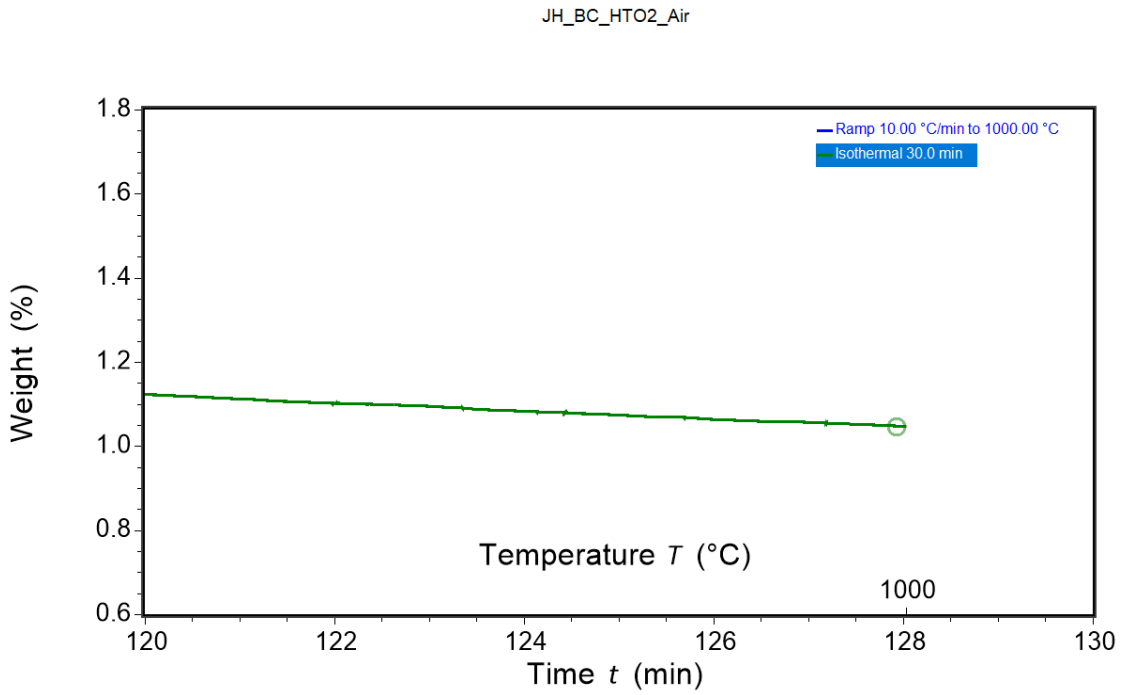

Figure 50. TGA results of Hydrogel 2.

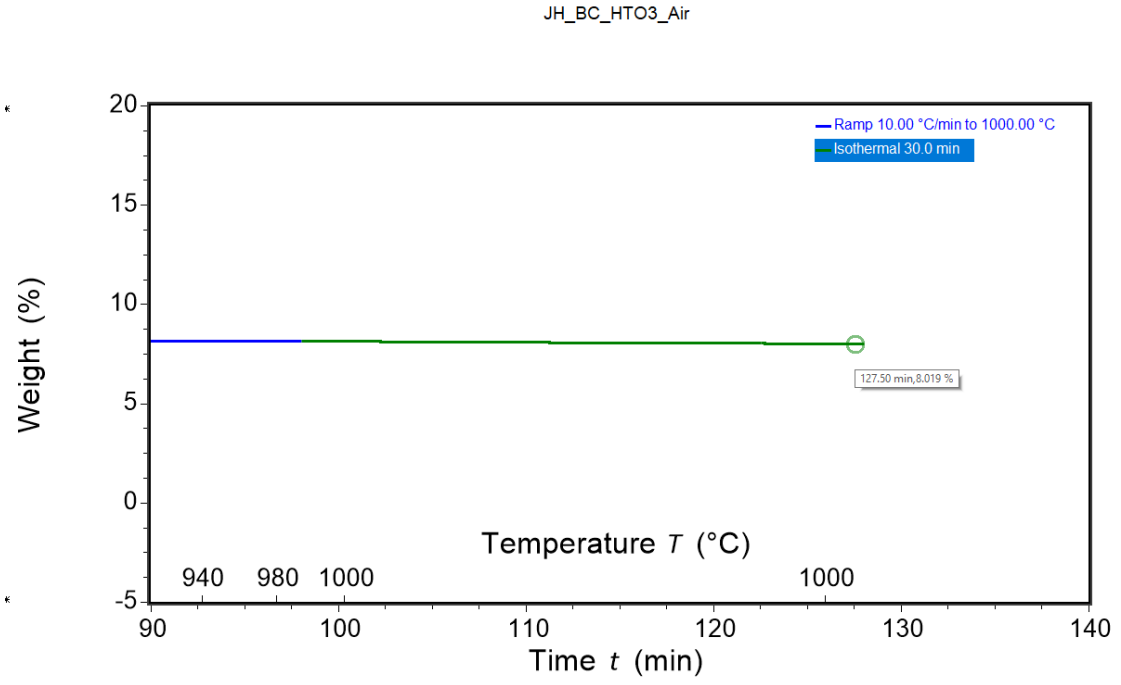

Figure 51. TGA results of Hydrogel 3.

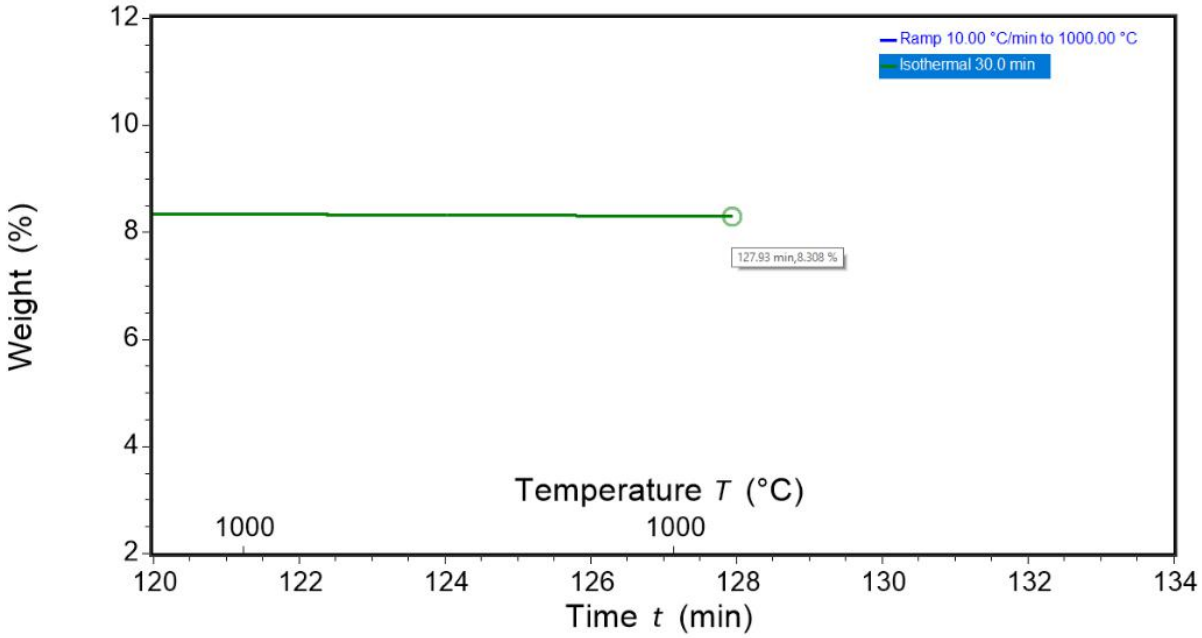

Figure 52. TGA results of Aerogel.

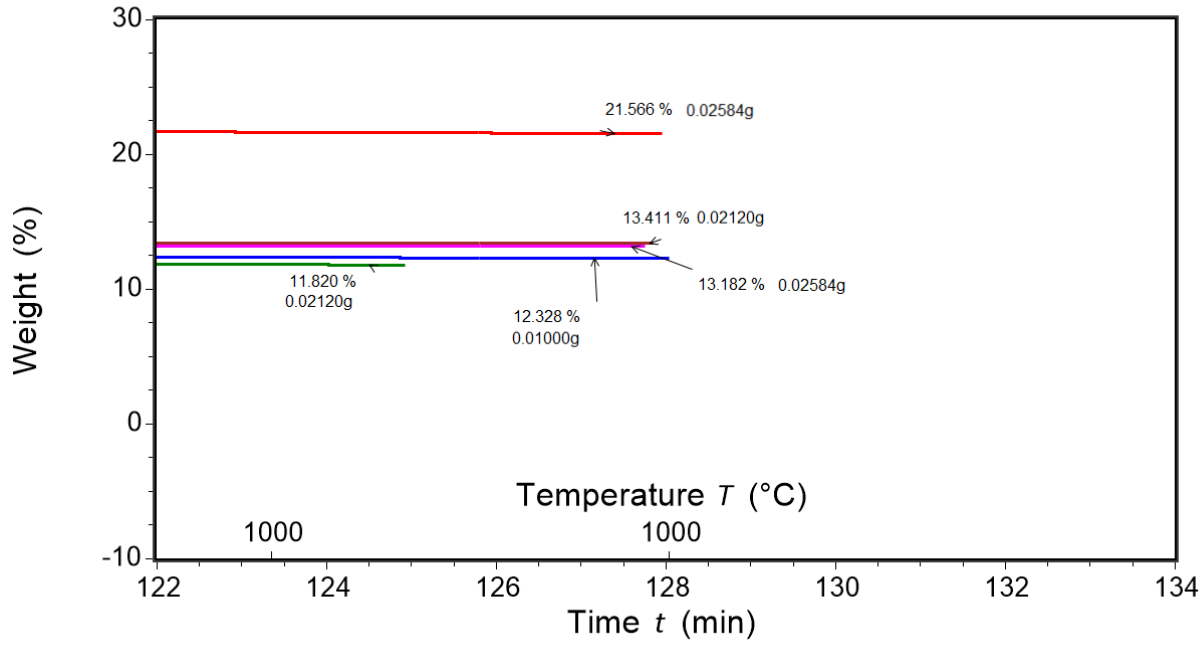

Figure 53. TGA results of different BC aerogel HTO composites with different HTO loadings.

Additionally, another active method was also done as a novel attempt to create a film. 2 g of BC pellicles was smashed with a house blender for 5 min with 100 mL of DI water to create a homogeneous solution. Then magnetically stirred at 200 RPM for 5 min with 0.01 g of HTO. The solution was poured into a metal pan and oven dried at 60^{o} C for 24 hours. The results were a thin piece of paper that easily disintegrated in water and was ill-suited for this application.

Figure 54. BC smashed with a house blender and mixed with HTO in an aluminum casting pan before oven drying at 60^{o} C for 24 hours.

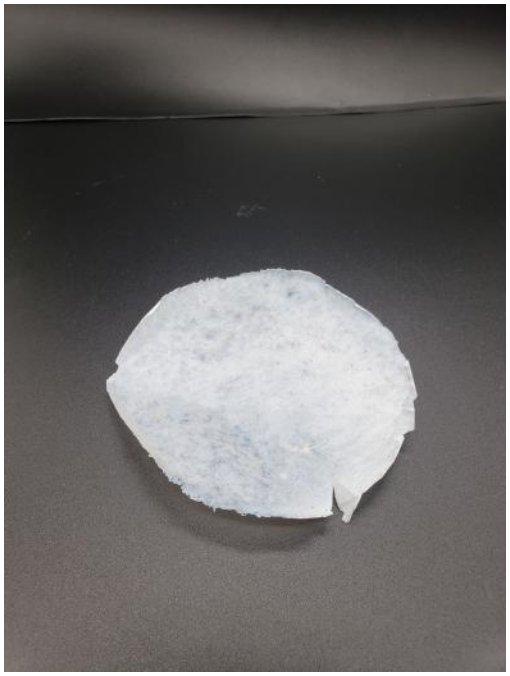

Figure 55. Results of smashed BC blended with HTO after oven drying.

The next step was to try and make BC aerogel composites with vacuum infiltration at different HTO concentrations. All variables were kept the same throughout the testing, this included HTO mixing conditions. One of the harder variables to keep consistent would be the porosity and density of the BC aerogel as a whole. Some areas would be thinner than others even though the BC freeze-dried came from the same batch of harvested BC. Different HTO concentrations for the BC aerogel were successfully made. The issue that came with this was the repeatability of making the composite the same consistent concentration for a specific concentration %. For example, attempting to make a batch 10 wt % HTO composite yielded some highly variable standard deviation between each sample. In addition, it seems like the method that the BC was frozen also played a minor role in the vacuum infiltration. From TGA data shown, it appears that BC frozen using liquid nitrogen have better results with HTO infiltration compared to those frozen in the freezer. There are still other factors to note that also

have an effect including seal between the BC and funnel, size of the freeze-dried BC, and posterity of the microstructure.

A third set of testing was done to see if a combination of infiltrating hydrogel then freeze drying it with liquid nitrogen would give more consistent results. One of the issues encountered when freezing with liquid nitrogen is that the BC composites turn brittle when compared to freezing in a freezer. Larger pieces of BC frozen using liquid nitrogen also tend to have cracks after freeze drying. The cracks are much less prominent in smaller pieces of BC. However the benefits of freezing with liquid nitrogen is that the BC maintains more of its porosity and thickness.

Another issue with larger pieces of freeze dried BC is that it's not forming a good enough seal between the filter paper and funnel itself. This is due to the uneven surface of the freeze dried BC along with the pressure of the vacuum spread over a larger area. One potential solution for this is to soak the BC first in water for 24 hours and trimming the piece to the shape of the funnel before attempting vacuum filtration. This is seen in sample 6. To note, sample 6 was done using BC frozen in the freezer.

Table 9. Overview of different BC samples infiltration methods. Adapted from [48].

Sample	Method
0	BC hydrogel was vacuum in HTO solution for 30 sec, frozen with liquid nitrogen then freeze-dried
1	BC hydrogel was vacuum filtered to remove excess water then vacuum in HTO solution for 30 sec, frozen with liquid nitrogen then freeze-dried
2	BC hydrogel was vacuum filtered to remove excess water then vacuum infiltrated with HTO solution, frozen with liquid nitrogen then freeze dried
3	BC aerogel passively soaked in HTO solution then air dried
4	BC hydrogel was vacuum filtered to remove excess water, passively soaked in HTO solution for 24-48 hours, air dried
5	BC hydrogel was passively soaked in HTO solution for 24-48 hours, vacuum filtered to remove excess water, frozen with liquid nitrogen then freeze dried
6	BC aerogel was vacuum filtered with HTO solution then air dried

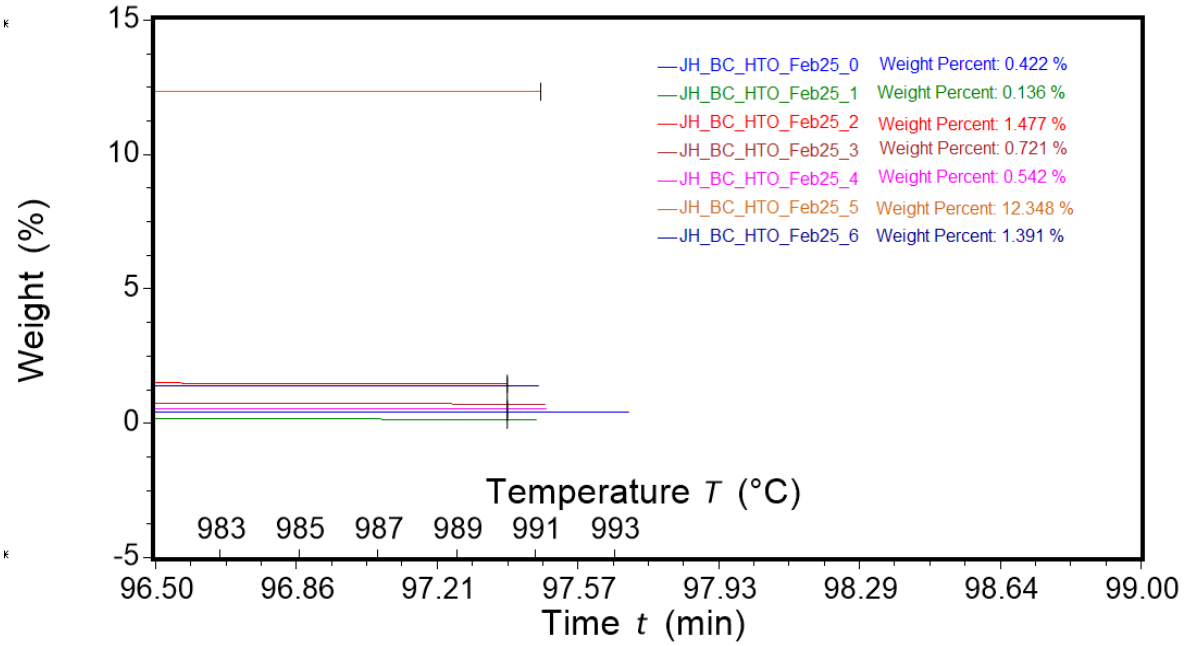

Figure 56. TGA results of samples from Table 9.

Figure 57. A 2.5 cm x 2.5 cm piece of liquid nitrogen frozen and freeze dried BC.

Figure 58. A 8 cm x 8 cm piece of liquid nitrogen frozen and freeze dried BC. Note the cracks that appear through the surface, causing issues with regular vacuum infiltration.

Figure 59. A 8 cm x 8 cm piece of freezer frozen and freeze dried BC. Note the thickness and that there are no cracks compared to liquid nitrogen frozen BC.

Figure 60. A 8 cm x 8 cm piece of liquid nitrogen frozen and freeze dried BC. Note the thickness compared to freezer frozen BC.

The next method tried was controlling the amount of HTO that is being infiltrated into the BC during vacuum filtering. A piece of BC, prior to freeze drying and approx. 8cm by 8 cm, is placed onto the funnel, with a piece of 20 micron filter paper between them. As the excess water is being filtered from the BC, sonicated HTO solution is placed drop wise with a disposable pipette onto the BC evenly and in a controlled manner. Then the BC composite frozen using liquid nitrogen is freeze dried. Vacuuming it first in the hydrogel state before liquid nitrogen also removes the brittleness as the porosity and thickness is reduced significantly. In theory, this should provide a more even distribution of the nanoparticles throughout the BC structure and in turn give more consistent results. Targeted HTO concentration was 10% weight concentration based on the wet weight of the BC pellicle.

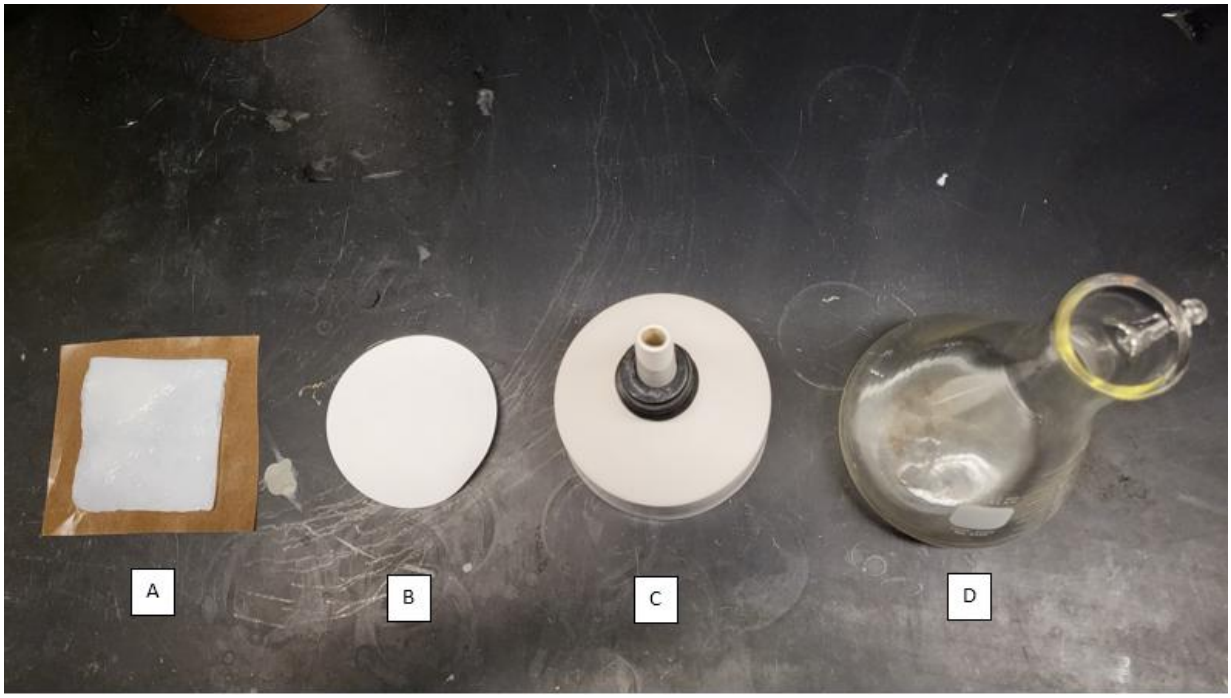

Figure 61. An overview of vacuum filtration setup for larger pieces of BC, (A) 8 cm x 8 cm BC hydrogel, (B) 2.5 micron filter paper, (C) ceramic filter funnel, (D) 1 L vacuum flask.

Figure 62. Overview of 8 cm x 8 cm of BC hydrogel placed in a funnel with a piece of 2.5 micron filter paper between them. Note that the hydrogel does not completely cover the funnel.

TGA results show that the HTO weight % concentration was approx. 1% meaning that very little of the particles were successfully infiltrated. SEM images show that the majority of the HTO remains on the surface of this BC. Also, when washing the BC after vacuum infiltration, the majority of the HTO particles that remained on the surface was cleaned off as evidenced by the clean DI water turning opaque. This again confirms the previous tests done on the smaller pieces of BC hydrogel that it was harder for the HTO particles to penetrate compared to freeze-dried BC. This poses a problem when scaling up with larger pieces of BC vs smaller pieces as done in previous tests. One potential issue is the HTO particles are not penetrating deep enough into the BC structure due to the hydrogel state.

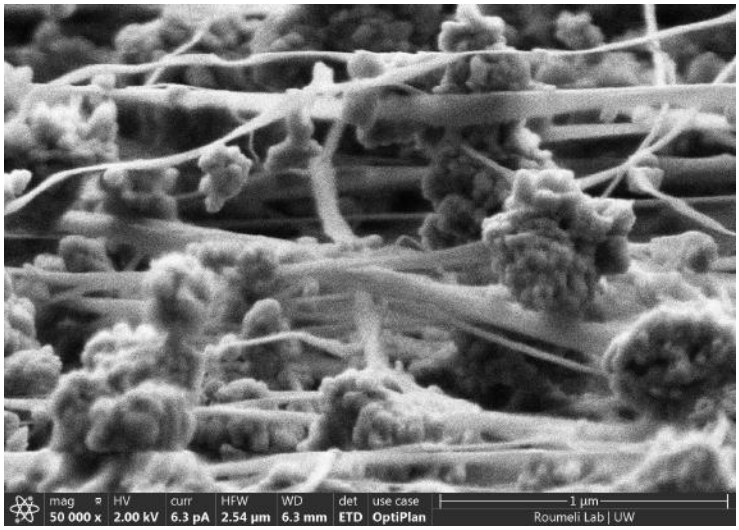

Figure 63. SEM image of 8 cm x 8 cm BC hydrogel with infiltrated HTO after freeze drying. Note that the HTO mainly remains on the surface of the hydrogel.

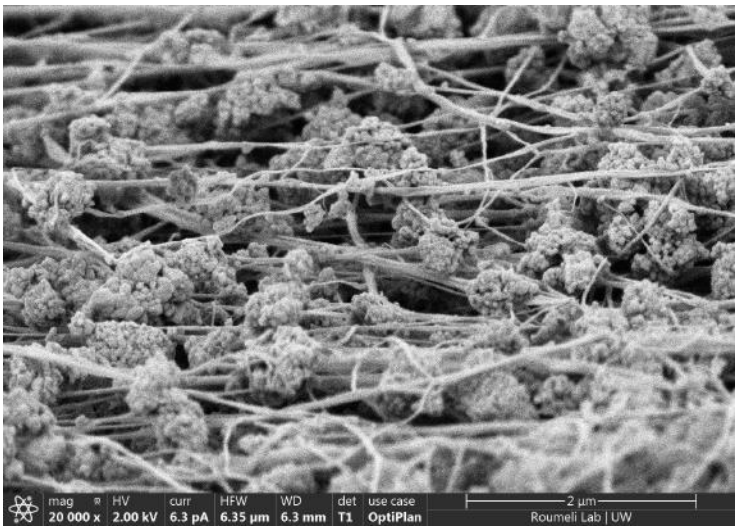

Figure 64. SEM image of 8 cm x 8 cm BC hydrogel with infiltrated HTO after freeze drying. Note that the HTO mainly remains on the surface of the hydrogel.

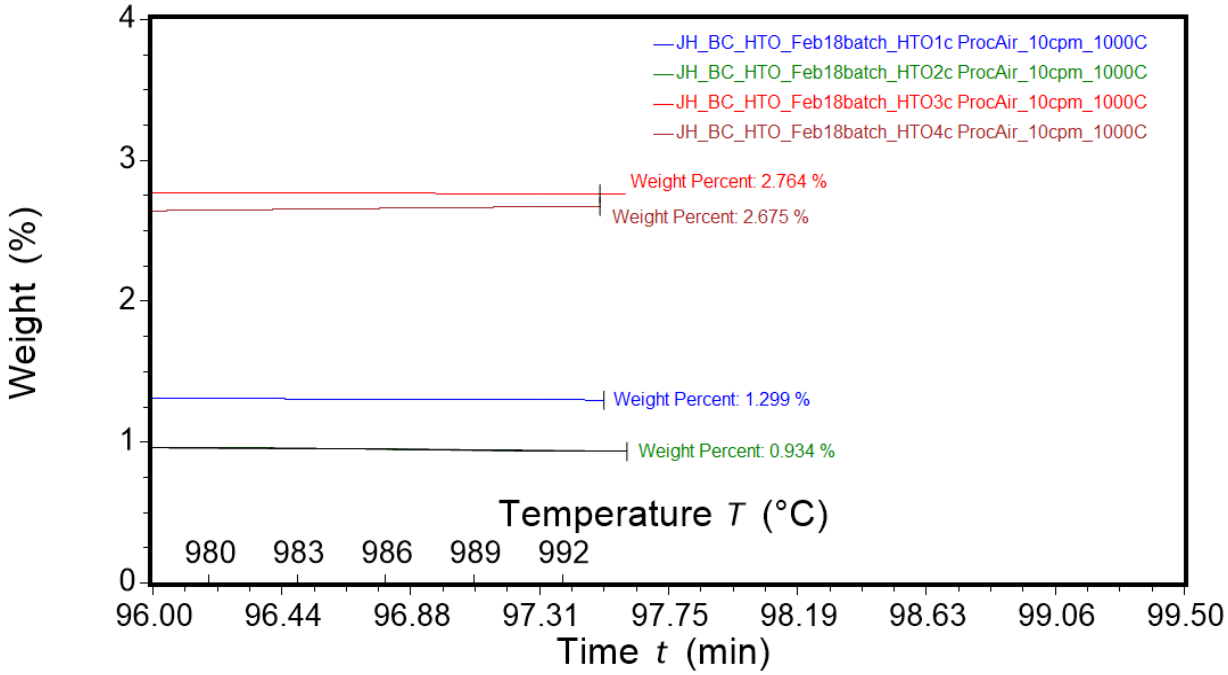

Figure 65. TGA results of 8 cm x 8 cm HTO BC hydrogel composites that were freezer frozen after infiltration and freeze dried. TGA tests done on center cut pieces.

Another attempt of combining both passive and active infiltration was made to see if it solved the deficiencies of particle infiltration with large pieces of freeze dried BC. A large piece of BC (8 cm x 8 cm) frozen using liquid nitrogen was soaked in the HTO solution (0.1g in 1000 mL of DI water) overnight then vacuumed to see if this had a better consistency with particle distribution in the BC microstructure. This was done with another batch of aerogels frozen using liquid nitrogen instead of freezing in the freezer. As seen in the TGA results, it seems like BC aerogel frozen using liquid nitrogen does produce better results, in terms of HTO infiltration, than the BC frozen with the freezer. This is most likely due to the increased porosity and volume compared to the non-liquid nitrogen BC aerogel. The unfortunate part is brittleness that induces cracks within the aerogel structure, meaning vacuum filtration (active infiltration) alone is not enough and a combination of active and passive is needed for successful infiltration of nanoparticles. To confirm that Sample 1-2 did have HTO infiltrated, another TGA test was run,

with promising results. It seems that sonication bathing the hydrogel before freeze drying increases porosity and thus makes it easier for the HTO particles to infiltrate in larger pieces of BC [49]. However this does bring up the issue that HTO weight % concentrations may not be consistent throughout.

Figure 66. Nitrogen frozen and freeze dried piece of BC. Note the irregular surface features of the nitrogen frozen BC that makes it difficult to vacuum filtrate by regular means.

Table 10. Overview of different batch of nitrogen frozen BC testing various infiltration methods.

Sample	Method
1-1	Soaked aerogel in water, vacuum filter with HTO solution, frozen in freezer, then freeze dried
1-2	Sonication bathed BC hydrogel, frozen with liquid nitrogen, freeze dried, passively soaked in HTO solution, vacuum filtered leftover solution, air dried
1-3	Sonication bathed BC hydrogel, frozen with liquid nitrogen, freeze dried, passively soaked in HTO solution, vacuum filtered leftover solution, frozen with liquid nitrogen, then freeze dried
1-4	BC aerogel passively soaked in HTO solution then air dried
1-5	Sonication bathed BC hydrogel, vacuumed in HTO solution overnight, frozen with liquid nitrogen, then freeze dried
1-6	BC aerogel was vacuum infiltrated with HTO solution then air dried

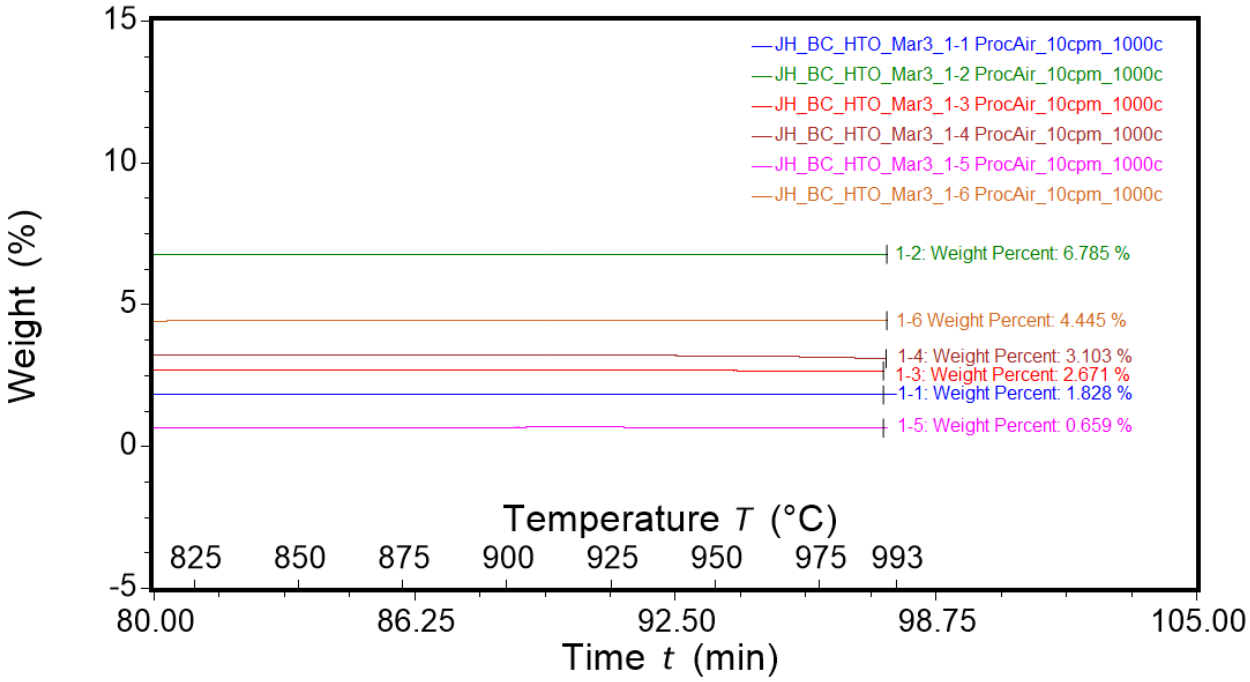

Figure 67. TGA results of samples from Table 10.

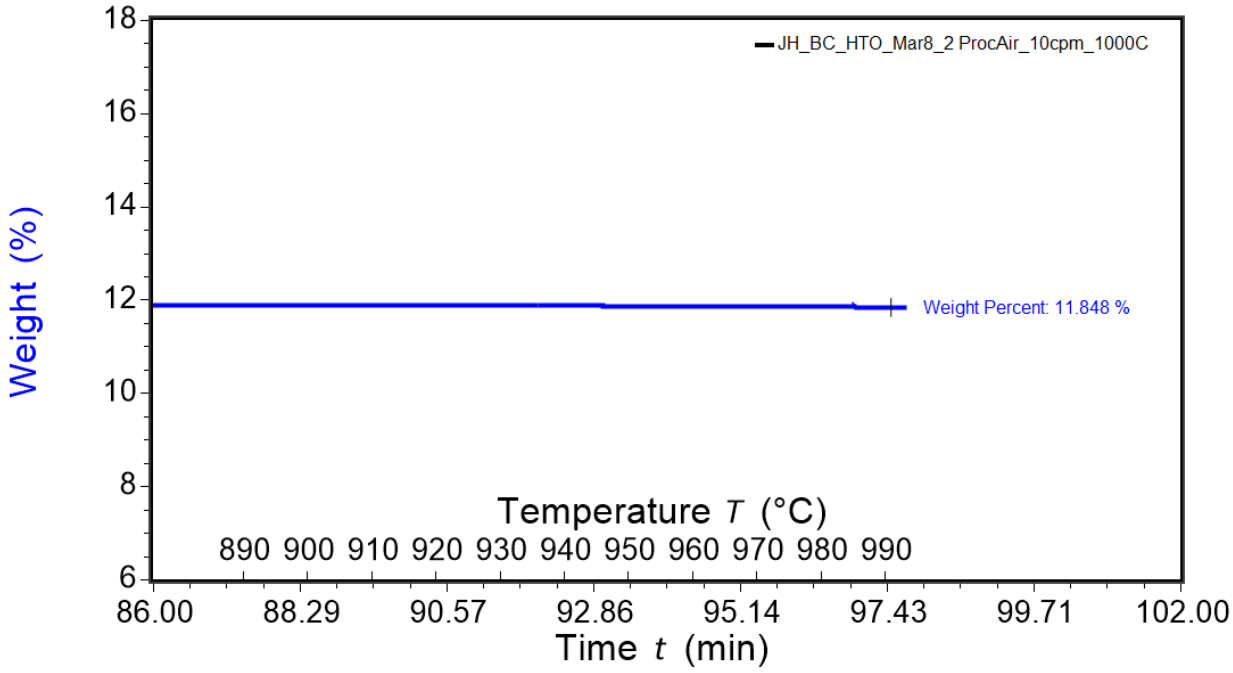

Figure 68. Second TGA test done on Sample 1-2 to confirm that HTO has infiltrated structure.

Note that the amount of HTO by weight % is more than the first test.

Another method explored was creating an aerogel with the HTO particles already mixed into the BC suspension before freeze-drying. The BC pellicle was cut into small pieces with scissors then smashed in a house blender for approx. 10 min. Then equally amounts DI water is added into the suspension along with the desired amount of HTO. The BC HTO suspension is probe sonicated at a amplitude of 75% for 1 hour under an ice bath to prevent overheating [50]. The sonicated suspension is then frozen with liquid nitrogen and freeze-dried in the same manner as all the other BC composites. The results turned out to be too delicate for use.

Figure 69. 3 different samples of BC based aerogels.

Chapter 4 - Conclusion

The goal of this research study was to examine a cellulose structure that would be a suitable scaffold as a composite infiltrated with HTO nanoparticles. We conducted a multi-purpose analysis focusing on the robustness, particle retention, ease of particle infiltration and scalability of the cellulose scaffold composites. The first step was to explore different cellulose types as a potential scaffold option, looking into both micro and nanocellulose types. We first experimented with synthesizing the cellulose scaffolds using a variety of methods including acid hydrolysis, TEMPO oxidation with mechanical defibrillation and fermentation. Only cellulose nanofibrils and bacterial cellulose were produced using TEMPO/mechanical defibrillation and fermentation, respectively. The first option explored was producing a hydrogel using microcrystalline cellulose, hydroxyethyl cellulose and cellulose nanofibrils. Only the cellulose nanofibrils were able to create the hydrogel structure we expected, however it was not

robust enough for our applications even though it survived the acid stability test. This left the bacterial cellulose as the only other viable cellulose scaffold.

Two forms of bacterial cellulose were explored, a hydrogel and aerogel state, with the aerogel state being the most favorable as it had better particle retention after multiple cycling tests and was easier to infiltrate with the more porous hierarchical nanostructure. On the smaller scale, using 2.5 cm diameter BC pellicles that have been frozen using either a freezer or liquid nitrogen then freeze dried, HTO infiltration was successful but not very consistent in terms of nanoparticle weight %. This is mainly due to the uneven and irregular natural density of the BC pellicles before and after freeze drying. A combination of SEM and TGA testings confirmed that the HTO particles were successfully infiltrated deep into the BC aerogel.

When trying to scale up the process using larger sheets of BC aerogel, approx 8 cm x 8 cm we encountered some issues in infiltrating the HTO particles. Several other methods were explored including vacuuming in the HTO solution, passive soaking with the aerogel, and smashing the BC in a blender with the HTO to make a different type of aerogel. Further testing showed that the best results with larger pieces of BC aerogel came from freezing the hydrogel with liquid nitrogen and using a combination of passive and active infiltration methods.

Chapter 5 – Future Work

As shown in previous testing, scaling to larger pieces of BC pellicles proved to be more difficult. In this regard, other novel methods should be explored such as in situ infiltration [51]. By growing the bacterial cellulose with the HTO, this should give more consistent results in terms of particle infiltration and potentially even better particle retention.

Tensile testing could be performed in the future on the BC composites, especially with different HTO weight % to see the effect of the particle amounts on the mechanical properties.

References

[1] S. Yang, F. Zhang, H. Ding, P. He, and H. Zhou, “Lithium metal extraction from seawater,” Joule, vol. 2, no. 9, pp. 1648–1651, 2018.

[2] X. Luo, K. Zhang, J. Luo, S. Luo, and J. Crittenden, “Capturing lithium from wastewater using a fixed bed packed with 3-D MnO2 ion cages,” Environ. Sci. Technol., vol. 50, no. 23, pp. 13002–13012, 2016.

[3] J. Luo, K. Fu, D. Yu, K. D. Hristovski, P. Westerhoff, and J. C. Crittenden, “Review of advances in engineering nanomaterial adsorbents for metal removal and recovery from water: Synthesis and microstructure impacts,” ACS EST Eng., vol. 1, no. 4, pp. 623–661, 2021.

[4] L. Tang et al., “Highly efficient, stable, and recyclable hydrogen manganese oxide/cellulose film for the extraction of lithium from seawater,” ACS Appl. Mater. Interfaces, vol. 12, no. 8, pp. 9775–9781, 2020.

[5] J. George and S. N. Sabapathi, “Cellulose nanocrystals: synthesis, functional properties, and applications,” Nanotechnol. Sci. Appl., vol. 8, pp. 45–54, 2015.

[6] Y. Habibi, L. A. Lucia, and O. J. Rojas, “Cellulose nanocrystals: chemistry, self-assembly, and applications,” Chem. Rev., vol. 110, no. 6, pp. 3479–3500, 2010.

[7] P. Bajpai, “Structure of Lignocellulosic Biomass,” in SpringerBriefs in Molecular Science, Singapore: Springer Singapore, 2016, pp. 7–12.

[8] Y. Su et al., “Fractional pretreatment of lignocellulose by alkaline hydrogen peroxide: Characterization of its major components,” Food Bioprod. Process., vol. 94, pp. 322–330, 2015.

[9] S. H. Zeronian and M. K. Inglesby, “Bleaching of cellulose by hydrogen peroxide,” Cellulose, vol. 2, no. 4, pp. 265–272, 1995.

[10] H. Zhang et al., “Ultrafast selective transport of alkali metal ions in metal organic frameworks with subnanometer pores,” Sci. Adv., vol. 4, no. 2, p. eaaq0066, 2018.

[11] D. Trache et al., “Nanocellulose: From fundamentals to advanced applications,” Front. Chem., vol. 8, p. 392, 2020.

[12] T. Abitbol et al., “Nanocellulose, a tiny fiber with huge applications,” Curr. Opin. Biotechnol., vol. 39, pp. 76–88, 2016.

[13] A. Gumrah Dumanli, “Nanocellulose and its Composites for Biomedical Applications,” Curr. Med. Chem., vol. 24, no. 5, pp. 512–528, 2017.

[14] G. K. Gupta and P. Shukla, “Lignocellulosic biomass for the synthesis of nanocellulose and its Eco-friendly advanced applications,” Front. Chem., vol. 8, p. 601256, 2020.

[15] A. Isogai, T. Saito, and H. Fukuzumi, “TEMPO-oxidized cellulose nanofibers,” Nanoscale, vol. 3, no. 1, pp. 71–85, 2011.

[16] C. Zhong, “Industrial-scale production and applications of bacterial cellulose,” Front. Bioeng. Biotechnol., vol. 8, p. 605374, 2020.

[17] Z. Li and Z. Lin, “Recent advances in polysaccharide‐based hydrogels for synthesis and applications,” Aggregate, vol. 2, no. 2, 2021.

[18] “Composite films - Purdue NanoForestry,” Purdue.edu. [Online]. Available: https://engineering.purdue.edu/nanotrees/composites.shtml. [Accessed: 12-Mar-2022].

[19] X. Xu, F. Liu, L. Jiang, J. Y. Zhu, D. Haagenson, and D. P. Wiesenborn, “Cellulose nanocrystals vs. cellulose nanofibrils: a comparative study on their microstructures and effects as polymer reinforcing agents,” ACS Appl. Mater. Interfaces, vol. 5, no. 8, pp. 2999–3009, 2013.

[20] C. Trilokesh and K. B. Uppuluri, “Isolation and characterization of cellulose nanocrystals from jackfruit peel,” Sci. Rep., vol. 9, no. 1, p. 16709, 2019.

[21] P. Lu and Y.-L. Hsieh, “Preparation and properties of cellulose nanocrystals: Rods, spheres, and network,” Carbohydr. Polym., vol. 82, no. 2, pp. 329–336, 2010.

[21] N. Grishkewich, N. Mohammed, J. Tang, and K. C. Tam, “Recent advances in the application of cellulose nanocrystals,” Curr. Opin. Colloid Interface Sci., vol. 29, pp. 32–45, 2017.

[22] L. Di Giorgio, L. Martín, P. R. Salgado, and A. N. Mauri, “Synthesis and conservation of cellulose nanocrystals,” Carbohydr. Polym., vol. 238, no. 116187, p. 116187, 2020.

[23] X. Yang, M. S. Reid, P. Olsén, and L. A. Berglund, “Eco-friendly cellulose nanofibrils designed by nature: Effects from preserving native state,” ACS Nano, vol. 14, no. 1, pp. 724–735, 2020.

[24] T. Yi et al., “From cellulose to cellulose nanofibrils-A comprehensive review of the preparation and modification of cellulose nanofibrils,” Materials (Basel), vol. 13, no. 22, p. 5062, 2020.

[25] O. Nechyporchuk, M. N. Belgacem, and J. Bras, “Production of cellulose nanofibrils: A review of recent advances,” Ind. Crops Prod., vol. 93, pp. 2–25, 2016.

[26] H. Jin, Y. Nishiyama, M. Wada, and S. Kuga, “Nanofibrillar cellulose aerogels,” Colloids Surf. A Physicochem. Eng. Asp., vol. 240, no. 1–3, pp. 63–67, 2004.

[27] “Microscopy and spectroscopy characterization of Eco-friendly composites and nanocomposites,” in Biopolymers and Biomaterials, Toronto ; New Jersey : Apple Academic Press, 2018.: Apple Academic Press, 2018, pp. 297–344.

[28] V. T. Nguyen, B. Flanagan, M. J. Gidley, and G. A. Dykes, “Characterization of cellulose production by a Gluconacetobacter xylinus strain from Kombucha,” Curr. Microbiol., vol. 57, no. 5, pp. 449–453, 2008.

[29] S. Swingler, A. Gupta, H. Gibson, M. Kowalczuk, W. Heaselgrave, and I. Radecka, “Recent advances and applications of bacterial cellulose in biomedicine,” Polymers (Basel), vol. 13, no. 3, p. 412, 2021.

[30] S.-P. Lin, I. Loira Calvar, J. M. Catchmark, J.-R. Liu, A. Demirci, and K.-C. Cheng, “Biosynthesis, production and applications of bacterial cellulose,” Cellulose, vol. 20, no. 5, pp. 2191–2219, 2013.

[31] S. Gorgieva and J. Trček, “Bacterial cellulose: Production, modification and perspectives in biomedical applications,” Nanomaterials (Basel), vol. 9, no. 10, p. 1352, 2019.

[32] C. Zhong, “Industrial-scale production and applications of bacterial cellulose,” Front. Bioeng. Biotechnol., vol. 8, p. 605374, 2020.

[33] R. Chitrakar, Y. Makita, K. Ooi, and A. Sonoda, “Lithium recovery from salt lake brine by H2TiO3,” Dalton Trans., vol. 43, no. 23, pp. 8933–8939, 2014.

[34] H. Qian et al., “HTO/cellulose aerogel for rapid and highly selective Li+ recovery from seawater,” Molecules, vol. 26, no. 13, p. 4054, 2021.

[35] C.-L. Yu et al., “The structure of H2TiO3-a short discussion on ‘Lithium recovery from salt lake brine by H2TiO3,’” Dalton Trans., vol. 44, no. 35, pp. 15721–15724, 2015.

[36] L. A. Limjuco et al., “H 2 TiO 3 composite adsorbent foam for efficient and continuous recovery of Li + from liquid resources,” Colloids Surf. A Physicochem. Eng. Asp., vol. 504, pp. 267–279, 2016.

[37] L. Zhang, D. Zhou, G. He, Q. Yao, F. Wang, and J. Zhou, “Synthesis of H2TiO3–lithium adsorbent loaded on ceramic foams,” Mater. Lett., vol. 145, pp. 351–354, 2015.

[38] C. P. Lawagon, G. M. Nisola, R. A. I. Cuevas, H. Kim, S.-P. Lee, and W.-J. Chung, “Development of high capacity Li+ adsorbents from H2TiO3/polymer nanofiber

composites: Systematic polymer screening, characterization and evaluation," J. Ind. Eng. Chem., vol. 70, pp. 124–135, 2019.

[39] X.-C. Shi, Z.-B. Zhang, D.-F. Zhou, L.-F. Zhang, B.-Z. Chen, and L.-L. Yu, "Synthesis of Li+ adsorbent (H2TiO3) and its adsorption properties," Trans. Nonferrous Met. Soc. China, vol. 23, no. 1, pp. 253–259, 2013.

[40] J. Gong, J. Li, J. Xu, Z. Xiang, and L. Mo, "Research on cellulose nanocrystals produced from cellulose sources with various polymorphs," RSC Adv., vol. 7, no. 53, pp. 33486–33493, 2017.

[41] A. Serra, I. González, H. Oliver-Ortega, Q. Tarrès, M. Delgado-Aguilar, and P. Mutjé, "Reducing the amount of catalyst in TEMPO-oxidized cellulose nanofibers: Effect on properties and cost," Polymers (Basel), vol. 9, no. 11, p. 557, 2017.

[42] A. S. Amarasekara, D. Wang, and T. L. Grady, "A comparison of kombucha SCOBY bacterial cellulose purification methods," SN Appl. Sci., vol. 2, no. 2, 2020.

[43] J. B. Mietner, X. Jiang, U. Edlund, B. Saake, and J. R. G. Navarro, "3D printing of a bio-based ink made of cross-linked cellulose nanofibrils with various metal cations," Sci. Rep., vol. 11, no. 1, p. 6461, 2021.

[44] H. Wei, K. Rodriguez, S. Renneckar, and P. J. Vikesland, "Environmental science and engineering applications of nanocellulose-based nanocomposites," Environ. Sci. Nano, vol. 1, no. 4, pp. 302–316, 2014.

[45] L. Valencia, S. Kumar, E. M. Nomena, G. Salazar-Alvarez, and A. P. Mathew, "In-situ growth of metal oxide nanoparticles on cellulose nanofibrils for dye removal and

antimicrobial applications," ACS Appl. Nano Mater., vol. 3, no. 7, pp. 7172–7181, 2020.

[46] V. Andree et al., "Influence of drying methods on the physical properties of bacterial nanocellulose," Mater. Res. Express, vol. 8, no. 2, p. 025402, 2021.

[47] J. Patiño-Masó, F. Serra-Parareda, Q. Tarrés, P. Mutjé, F. X. Espinach, and M. Delgado-Aguilar, "TEMPO-oxidized cellulose nanofibers: A potential bio-based superabsorbent for diaper production," Nanomaterials (Basel), vol. 9, no. 9, p. 1271, 2019.

[48] J. He et al., "Superelastic and superhydrophobic bacterial cellulose/silica aerogels with hierarchical cellular structure for oil absorption and recovery," J. Hazard. Mater., vol. 346, pp. 199–207, 2018.

[49] H. Abral, V. Lawrensius, D. Handayani, and E. Sugiarti, "Preparation of nano-sized particles from bacterial cellulose using ultrasonication and their characterization," Carbohydr. Polym., vol. 191, pp. 161–167, 2018.

[50] C. Li, Z.-Y. Wu, H.-W. Liang, J.-F. Chen, and S.-H. Yu, "Ultralight multifunctional carbon-based aerogels by combining graphene oxide and bacterial cellulose," Small, vol. 13, no. 25, p. 1700453, 2017.

[51] F. Guan and C. F. Guo, "Flexible, high-strength, and porous nano-nano composites based on bacterial cellulose for wearable electronics: a review," Soft Science, vol. 1, no. 3, p. 16, 2021.